https://doi.org/10.5194/egusphere-2026-869
Preprint. Discussion started: 9 April 2026
© Author(s) 2026. CC BY 4.0 License.

Lake-Mountain synergy in convective clouds and precipitation over the Tibetan Plateau: a large-eddy simulation study

Kai Yang[1], Jinghua Chen[1], Tianliang Zhao[1, 3], Xiangde Xu[2], Chunsong Lu[1], Shizuo Fu[4], Yuehan Luo[1], Qingjian Yang[5], Ziqian Liu[1], Zhikuan Li[1], Lin Wu[1], Yuxiang Jin[1]

[1]State Key Laboratory of Climate System Prediction and Risk Management, China Meteorological Administration Aerosol-Cloud and Precipitation Key Laboratory, Nanjing University of Information Science & Technology, Nanjing, China, 210044
[2]State Key Laboratory of Severe Weather, Chinese Academy of Meteorological Sciences, Beijing 10081, China
[3]Wenjiang National Climatology Observatory, Chengdu, Sichuan 611135, China
[4]Key Laboratory for Humid Subtropical Eco-Geographical Processes of the Ministry of Education, Fujian Normal University, Fuzhou, China
[5]National Meteorological Information Center, China Meteorological Administration, Beijing, 100081, China

Correspondence to: Tianliang Zhao (tlzhao@nuist.edu.cn); Jinghua Chen (jhchen@nuist.edu.cn)

Abstract. Idealized large-eddy simulations (LES) are used to examine lake-mountain effects on clouds and precipitation over the Tibetan Plateau (TP) under conditions of low air density and limited moisture. This study conducts LES respectively with lake-only, mountain-only, and combined lake-mountain configurations. The alpine lake alleviates key constraints on convective organization by enhancing low-level moisture and reducing thermodynamic inhibition to convective initiation. However, in this energy- and moisture-limited environment, the lake alone induces only shallow ascent, sustaining shallow convection and weak precipitation with limited deepening. By contrast, mountain alone provides mechanically forced uplift, but the overall scarcity of moisture over the TP confines precipitation to a narrow area near the mountain. With combined lake-mountain configurations, lake-supplied moisture is lifted by the downstream mountain, deep convective clouds develop, yielding strong and extensive precipitation. Notably, mountains exhibit a reversed role in lake-mountain interactions affecting clouds and precipitation processes, owing to the competition between orographic lifting and blocking effects. High mountains enhance precipitation on the upstream side while suppressing downstream development by restricting low-level moisture transport from lake source, whereas low mountains allow broader horizontal moisture advection but induce weaker vertical development. Overall, lake-mountain coupling is intrinsic to the TP's high-elevation, moisture and energy limited environment, where lake-driven moistening lowers initiation barriers, orographic lifting and blocking organize and deepen convection, and mixed-phase processes further reshape precipitation patterns, a pathway that is typically not dominant over the plains. These findings clarify how high-elevation surface heterogeneity affects clouds and precipitation, with implications for the Asian water cycle.

1 Introduction

As the world's highest and most extensive plateau, the Tibetan Plateau (TP) exerts strong thermal and dynamical forcing on the atmosphere, shaping regional circulation and moisture transport through its interactions with the Asian monsoon systems and the midlatitude westerlies (Liu et al., 2007; Wu et al., 2015; Xu et al., 2008; Ye, 1981). The unique topography and geomorphology support widespread glaciers, permafrost, and alpine lakes (Yao et al., 2012; Zhang et al., 2014). These features underpin its designation as "the Third Pole" and "the Asian Water Tower" (Qiu, 2008; Xu et al., 2008), which sustains downstream ecosystems and water supplies for billions of people. As a climatically sensitive region, the Asian water tower is

https://doi.org/10.5194/egusphere-2026-869
Preprint. Discussion started: 9 April 2026
© Author(s) 2026. CC BY 4.0 License.

extremely vulnerable to climate change (Immerzeel et al., 2010; Yang et al., 2011). Rapid warming and cryospheric degradation during recent decades (Kang et al., 2010) have been associated with changes in water availability and an intensified hydrological cycle, contributing to glacier retreat and increasing variability in seasonal water supply (Huss and Hock, 2018; Li et al., 2022b). A central link in this chain is the cloud and precipitation process. In such cold, elevated environments, frequent phase transitions among solid, liquid and gas states result in rapid changes in regional water resources and energy balance, compounding the risks of water resource imbalance and hydrological extremes (Kang et al., 2010; Yao et al., 2022; Zhang et al., 2019).

Cloud microphysical processes regulate the conversion of condensate to precipitation and, in turn, influence the structure and evolution of convective systems. Satellite radar and simulation studies suggest that summer mesoscale convective systems over the TP tend to occur frequently but are typically weaker and smaller than their counterparts over the ocean and other continental regions (Fu et al., 2006; Luo et al., 2011; Qie et al., 2014). Over the TP, deeply precipitating convection is sporadic and often depends on localized forcing, suggesting that convection initiation can be more limiting than the magnitude of instability alone, making the “popcorn-like” cumulus clouds in summer (Li et al., 2016; Xu et al., 2002; Yang et al., 2024). This initiation barrier is consistent with the high elevation background, where the atmosphere is commonly limited in moisture and convective inhibition, making it difficult to overcome without focused lifting. The high elevation, low air density environment favors a deep, turbulent boundary layer and strong thermally driven circulations over the complex terrain, which can generate short lived but intense pockets of ascent even when large-scale conditions appear only weakly favorable (Xu et al., 2023; Yang et al., 2004). Once such localized ascent succeeds in eroding or penetrating the cap, shallow cumulus can deepen rapidly, producing brief episodes of vigorous vertical development, active precipitation formation, and intense rainfall (Chen et al., 2021). Yet the same moisture-limited setting also constrains convection maintenance, so convection over the TP often remains small and isolated, with limited horizontal extent and short lifetimes (Hu et al., 2016; Zheng et al., 2023). In this setting, surface heterogeneity (e.g., lake-land contrasts, snow/ice, grassland-barren transitions, and complex terrain) likely plays a more active dynamical role than in the lowlands by sharpening boundary-layer convergence and localized lifting, thereby triggering convection that would otherwise remain inhibited.

Land-atmosphere interactions over heterogeneous surfaces can profound influences on mesoscale and microscale atmospheric processes, modulating cloud formation and precipitation (Chen et al., 2020b; Kalthoff et al., 2009; Xiao et al., 2018). Surface heterogeneity often matters for convection not because it directly “creates Convective Available Potential Energy (CAPE)” but because it organizes the boundary layer into preferred lifting locations. Wet-dry patches, land-water boundaries, and heterogeneous land-cover patterns modify sensible and latent heat fluxes, shaping boundary depth and the horizontal gradients of temperature and moisture. These gradients can drive mesoscale circulations and sharpen convergence lines, providing focused ascent that helps parcels approach saturation and, when inhibition is weak enough, reach their Lifted Condensation Level (LCL) and sometimes their Level of Free Convection (LFC) (Chen and Avissar, 1994; Kalthoff et al., 2009). Observations and modeling further show that convection initiation frequently clusters along such heterogeneity-driven

https://doi.org/10.5194/egusphere-2026-869
Preprint. Discussion started: 9 April 2026
© Author(s) 2026. CC BY 4.0 License.

boundaries, and that cloud and precipitation evolution depends on the difference and persistence of the associated thermodynamic features (Frye and Mote, 2010; Lee et al., 2019; Rieck et al., 2014).

Land-lake configurations represent a prominent form of heterogeneity. The lake-land thermal contrast drives lake-breeze circulations that reorganize low-level convergence and can modulate local precipitation patterns (Henderson-Sellers, 1986; Laird et al., 2003). Lake breezes vary with season and diurnal heating, and over large water bodies, they can initiate deep convection when the lake-breeze front intensifies and provides strong lifting (Kristovich and Steve, 1995; Sills et al., 2011; Wang et al., 2019). Due to the enhanced heat capacity of water bodies (Biggs and Graves, 1962), lakes exhibit delayed warming and cooling compared to land surfaces. The lake remains relatively warm in a cooling environment, such as during night and winter, which is most notably associated with lake-effect snow (Kristovich et al., 2017; Peace and Sykes, 1966). Additionally, summertime lake breezes generate numerous other phenomena due to the stronger land surface heating and more abundant water vapor supply (Estoque et al., 1976; Lyons, 1972; Lyons and Cole, 1973). Both circulations can exert opposite effects on cloud patterns, reflecting the locations of the ascending and descending branches of the breeze circulation (Keen and Lyons, 1978). Much of this understanding derives from low-altitude, midlatitude regions such as the North American Great Lakes. In contrast, TP lakes are embedded in a high altitude, low density environment with strong surface-atmosphere coupling (Chen et al., 2017, 2020c), which may fundamentally alter the structure of lake-induced circulations and their capacity to trigger convection (Rüthrich et al., 2015; Wu et al., 2019; Yao et al., 2021, 2023).

Observational and modeling studies have provided growing evidence of such lake-atmosphere interactions across the TP. On the one hand, lakes on the TP exhibit substantial evaporation rates and serve as important sources of atmospheric water vapor, contributing significantly to the regional moisture budget (Wang et al., 2019, 2020a), providing the basic conditions for the cloud-precipitation process. On the other hand, strong thermal gradients arising from lake-land interactions can generate lake breezes, whose convergence induces vigorous upward motion and serves as a key trigger for deep convective systems in the region (Wang et al., 2019). Satellite observations show systematically enhanced morning cloud cover over lakes relative to adjacent land, consistent with lake-land thermal contrasts (Rüthrich et al., 2015). In the TP interior, elevated lake surface temperatures have been associated with enhanced convective precipitation, emphasizing the contribution of lake-induced moisture transport to local rainfall regimes (Zhang et al., 2016). Using satellite data and numerical simulations, Yao et al (2021, 2023) further showed that reduced sensible heat flux over lake surfaces relative to surrounding terrain drives lake-land breezes that organize subsidence over lake centers and ascent along lake margins, producing characteristic “cloud holes” and “cloud rings” that directly reflect the breeze circulation.

Because glacial erosion can create over-deepened basins that later fill with meltwater during retreat, alpine lakes often occur with mountainous terrain over the TP (Fig. S1) (Haeberli et al., 2016; Linsbauer et al., 2016). When lakes interact with surrounding topography, lake breezes can couple with valley winds and local circulations to strengthen local lifting and modulate heat and moisture transport (Barros et al., 2000; McGowan et al., 1995; Singh and Nakamura, 2009; Xu et al., 2021). Under favorable conditions, lake breezes were shown to destabilize the lower troposphere and trigger deep convection (Su et al., 2020), with downstream mountains amplifying the lake’s impact (Zhao et al., 2022). Yet the lake breeze structure is

https://doi.org/10.5194/egusphere-2026-869
Preprint. Discussion started: 9 April 2026
© Author(s) 2026. CC BY 4.0 License.

inherently narrow (Khodayar Pardo, 2015; Wood et al., 1999), current mesoscale numerical weather prediction (NWP) models remain insufficient to fully resolve micro and mesoscale structures responsible for initiating moist convection (Dehghan et al., 2018; Rousseau-Rizzi et al., 2017; Warren et al., 2014). Thus, sub-kilometer resolution is often required to capture lake-terrain interactions and the associated thermodynamics, motivating the use of large-eddy simulation (LES) to isolate the underlying physical mechanisms.

Despite growing recognition of lake-induced effects on atmospheric processes, the combined influence of lake-terrain interactions on convective development over the TP remains poorly constrained. Clarifying how lake moistening interacts with orographic lifting and blocking across different terrain heights is essential for improving hydroclimatic projections over the TP. Here, we explicitly treat mountain height as a control parameter and conduct a set of idealized LES sensitivity experiments in which the downstream terrain is changed. The following sections describe the experimental design, including model configuration and initial conditions (Sect. 2). Sect. 3 and Sect. 4 investigate the thermodynamic and microphysical mechanisms under different lake-terrain configurations and topographic heights. Sect. 5 synthesizes the findings and discusses their broader implications for lake-terrain coupled convection over the TP.

2 Model configuration and datasets

2.1 Model configuration

Numerical simulations were conducted using the Cloud Model 1 (CM1) version 21.1 (McGowan et al. 1995; Barros et al. 2000; Singh and Nakamura 2009), a non-hydrostatic, fully compressible cloud model designed for idealized studies of atmospheric phenomena, such as tropical cyclones, thunderstorms, and topographic gravity waves. In this study, we conducted a series of idealized simulations along a cross-section through the Nam Co Basin, to further understand the physical processes involved in the generation of mesoscale circulation and convection initiation driven by the synergistic effects of the lake and surrounding mountains (Fig. 1a). Land cover characteristics were derived from the MCD12C1 Production (Sulla-Menashe and Friedl, 2018), with grassland assigned to lowland areas and snow cover specified over mountainous terrain in summer (Fig. 1b). When large-scale atmospheric forcing is weak or absent, circulation within the basin is primarily driven by the thermally induced lake breeze and mountain-valley circulation. Hence, a cross-sectional transect over smoothed terrain, passing through Nam Co Lake and the Nyenchen Thanglha Mountain, was selected as the reference for the experimental design to investigate the associated thermal and dynamical characteristics (Fig. 1c-d).

The model was configured to solve the fully compressible governing equations on a three-dimensional domain of size 275 km×20 km×8 km (x, y and z dimensions, respectively) with a horizontal grid spacing of 100 ×100 m^2 and an adaptive timestep initialized suitable value of 1 s (Fig. 2). The terrain-following vertical grids were stretched (Wilhelmson and Chen, 1982) with constant vertical spacing of 100 m below 4 km and 400 m from 6 km to 8 km, resulting in a total of 53 levels. In the default configuration, the model operates in large eddy simulation (LES), and a fifth-order WENO scheme was employed for the advection of both scalars and momentum (Jiang and Shu, 1996). Since the simulations span a few hours and a relatively

https://doi.org/10.5194/egusphere-2026-869
Preprint. Discussion started: 9 April 2026
© Author(s) 2026. CC BY 4.0 License.

small domain, the Coriolis force has a negligible impact on cloud and precipitation processes, consistent with previous idealized terrain studies (Feldmann et al., 2024; Katona and Markowski, 2021). Physical parameterizations included the 1.5-order turbulent kinetic energy (TKE) closure scheme for subgrid-scale turbulence (Deardorff, 1980), with vertical turbulence tendencies calculated implicitly using the Crank-Nicholson scheme. The Klemp-Wilhelmson compressible pressure solver (Klemp and Wilhelmson, 1978) and the Morrison double-moment moisture scheme (Morrison et al., 2005) were employed. The revised land surface scheme developed for the Weather Research and Forecasting (WRF) model is also applied (Jiménez et al., 2012).

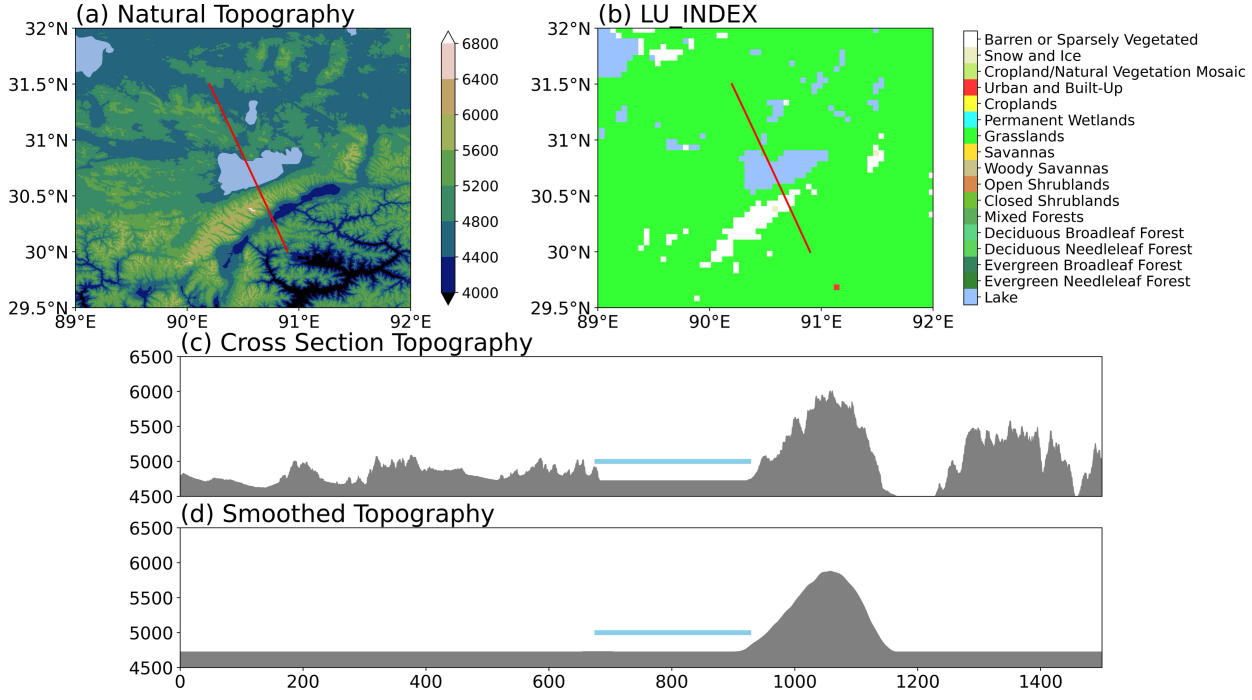


Figure 1. Configuration of the idealized cross-sectional simulations. The red transect line passes through Nam Co Lake and the Nyenchen Thanglha Mountains, (a) incorporating realistic topography from SRTM and (b) land cover from MCD12C1. (c) Cross-sectional topography is extracted along this line. (d) The smoothed version is used in the simulations to isolate thermal and dynamical responses associated with the typical lake-mountain configuration.

https://doi.org/10.5194/egusphere-2026-869
Preprint. Discussion started: 9 April 2026
© Author(s) 2026. CC BY 4.0 License.

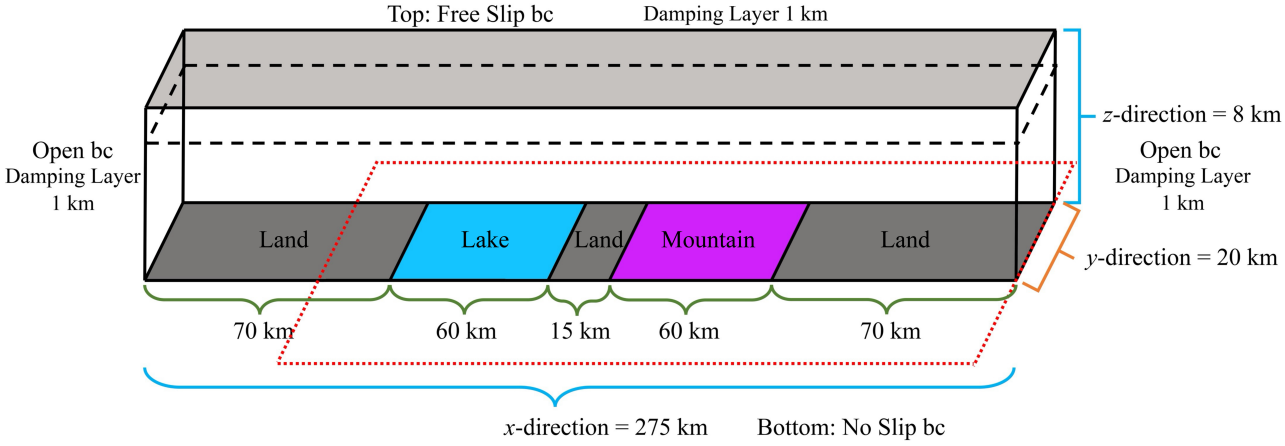


Figure 2. Domain configuration sketches of heterogeneous underlying surfaces. The blue and purple domains represent the lake and mountain, respectively. The different sizes of the lake are marked. The areas in red boxes are areas analyzed and reported.

2.2 Lake and Mountain geometries

Six sensitivity experiments were conducted based on the model configuration (detailed in Table 1) to examine the interactions between the lake and mountains of varying heights, assess the contributions of lake breeze and mountain-valley circulation, and investigate cloud-precipitation processes associated with the lake and surrounding topography.

Table 1. Lake and topography configuration for each simulation.

Name	Topography	Lake
LM-1500 (Lake+Mountain)	1500m-peak	Open Lake
LM-3000 (Lake+Mountain)	3000m-peak	Open Lake
LM-750 (Lake+Mountain)	750m-peak	Open Lake
OL (Only Lake)	None	Open Lake
OM (Only Mountain)	1500m-peak	None
NLM(No Lake+Mountain)	None	None

In the model configuration, simulations incorporating both lake and topography are oriented along the *x-direction* of the domain (see the cross-sections in Fig. 2d). Periodic boundary conditions are applied in the lateral boundary (*y-direction*), while an open-radiative boundary condition is imposed along the (*x-direction*) horizontal boundary to minimize wave reflection (Klemp and Wilhelmson, 1978). Consequently, the geometry of the open lake (x = 70-130 km) is effectively infinitely long in the *y-direction* because of the use of periodic flow-parallel lateral boundary conditions. This configuration has been shown to support the initiation of open-cell convection and lake-effect precipitation induced by the open lake (Gowan et al., 2021,

https://doi.org/10.5194/egusphere-2026-869
Preprint. Discussion started: 9 April 2026
© Author(s) 2026. CC BY 4.0 License.

2022). Based on the observed water temperature at a depth of 6 m in Nam Co, which was used as a proxy for surface temperature by Wang et al (2020), the lake surface temperature was set to 284 K (10.85 °C) in the model.

The terrain configuration is intended to provide insight into downstream processes that occur where lake-effect systems interact with lower terrain features. The "bell-cosine" terrain profile, which is used to investigate hill effects in large-eddy simulations (Xue and Giorgetta, 2021), is incorporated into the idealized model and defined by the following equation:

$$z_t = \frac{H}{2}\left(1 + cos\left(\frac{2\pi}{4L}(x - x_c)\right)\right), \quad (1)$$

Where H is the maximum hill height (1500 m) (set for control experiment: LM-1500), L is the half-width of the terrain (15 km) and x_c represents the ridge center location (175 km). An idealized bell-shaped mountain defined by the cosine profile was employed to ensure smooth curvature and continuous derivatives across the terrain. This configuration minimizes numerical artifacts, such as wave reflection or artificial convergence near sharp gradients, while providing a controlled, symmetric topographic forcing suitable for isolating orographic effects on atmospheric processes. We initialized the land surface with a temperature of 300 K (26.85 °C), and the soil temperature to 285 K (11.85 °C). To represent the observed cooling of terrain surfaces with altitude, the surface temperature over the mountain was prescribed to decrease linearly with height at a fixed lapse rate of 6.5 K km^{-1}.

2.3 Environmental conditions

Rather than optimizing parameterization schemes to reproduce real atmospheric conditions, our simulation intended to emphasize land-atmosphere interactions over the underlying surface of the lake and mountain, and to explore the change in convection initiation and cloud-precipitation processes over the TP. The initial profiles of potential temperature and water vapor mixing ratio used in this study were derived from radiosonde observations at the Naqu Station, whose atmospheric conditions are similar to those over Nam Co Lake, on August 14, 2023, at 00:00 UTC. It was a sunny day and the extensive low stratus cloud with a vertical extent of several hundred meters persisted over Nam Co Lake, and the initial sounding profile is shown in Fig. 3. The convective available potential energy (CAPE) was 392.94 J kg^{-1}, and the convective inhibition (CIN) was - 44.01 J kg^{-1}, indicating a favorable condition for convection initiation.

We initialized the simulations using the RKW-type wind profile (Rotunno et al., 1988), in which the u-component of the wind increases from 0 m s^{-1} at the surface to 15 m s^{-1} at the model top. As noted earlier, such winds are maintained at the inflow boundary using Rayleigh damping. The simulations were integrated for 20 h, with model output saved every 5 minutes.

https://doi.org/10.5194/egusphere-2026-869
Preprint. Discussion started: 9 April 2026
© Author(s) 2026. CC BY 4.0 License.

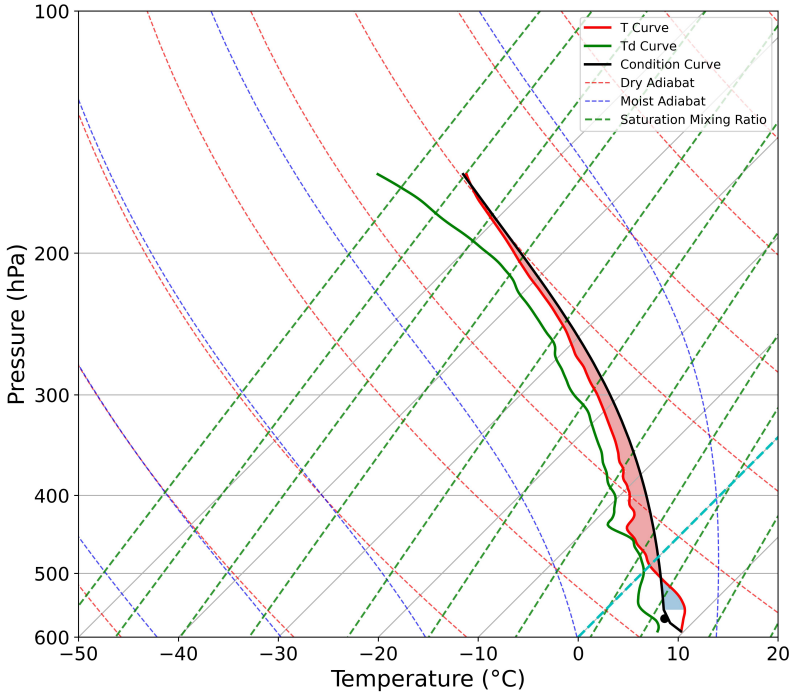


Figure 3. Skew T-lnp diagram illustrating the thermodynamic profile used to initialize all simulations.

2.4 Analysis methods

2.4.1 Phase-averaged decomposition

Phase-averaged analysis helps separate heterogeneity-induced circulations from random turbulent motions over heterogeneous surfaces. To isolate heterogeneity-induced circulations by removing the influence of background winds and isolating the perturbations caused by local surface features, we perform a phase-averaging decomposition along the periodic *y*-direction:

$$\phi = \langle \phi \rangle + \phi' , \quad (2)$$

Here, $\langle \phi \rangle$ denotes the horizontal averaged component of ϕ' and ϕ represents turbulent fluctuation. The following section decomposes horizontal wind and temperature fields to remove background contributions and analyze moist convection induced by lake-mountain interactions.

2.4.2 Hydrometeor and Precipitation mixing ratio tendencies

To investigate the modulating effects of lake-mountain interactions on cloud-precipitation processes, hydrometeor phase transitions and precipitation formation are quantified according to Gowan et al (2021, 2022). The surface precipitation mass

https://doi.org/10.5194/egusphere-2026-869
Preprint. Discussion started: 9 April 2026
© Author(s) 2026. CC BY 4.0 License.

flux rate, denoted as $\overline{P_{\mathrm{m}}}$, is defined to represent the temporal evolution of precipitation intensity, averaged over the central 15 km of the domain in the y-direction:

$$\overline{P_{\mathrm{m}}}(x) = \frac{\Delta P_m}{\Delta t}, \tag{3}$$

Where, $\overline{P_{\mathrm{m}}}$ (unit: kg s^{-1}) represents the accumulated precipitation mass over a time interval Δt.

Along-band cross-sections of the total hydrometeor mixing ratio, $\bar{q}$, and its phase-change-induced tendency, $\overline{q_{\mathrm{ten}}}$, are analyzed, both averaged with Equation 3. The total hydrometeor mixing ratio is given by:

$$\bar{q} = \bar{q}_c + \bar{q}_r + \bar{q}_i + \bar{q}_g + \bar{q}_s, \tag{4}$$

$$\overline{q_{\mathrm{ten}}} = \frac{\overline{\Delta q}}{\Delta t}, \tag{5}$$

where $\bar{q}_c$, $\bar{q}_r$ $\bar{q}_i$, $\bar{q}_g$, and $\bar{q}_s$ (unit: kg·kg^{-1}) represent the mixing ratios of cloud water, rain, ice, graupel, and snow, respectively. $\overline{q_{\mathrm{ten}}}$ (unit: kg·kg^{-1}·s^{-1}) denotes the tendency of total hydrometeor mixing ratio over a time interval Δt driven by phase changes. To further analyze $\overline{q_{\mathrm{ten}}}$, the vertically integrated total hydrometeor mass growth rate $\overline{Q_{\mathrm{growth}}}$ and mass loss rate $\overline{Q_{\mathrm{loss}}}$ are computed as functions of x-direction. Specifically, $\overline{Q_{\mathrm{growth}}}$ and $\overline{Q_{\mathrm{loss}}}$ are given by:

$$\overline{Q_{\mathrm{growth}}}(x) = \int_{z_s}^{z_t} \rho_d \overline{q_{\mathrm{ten\ pos}}}(x,z)dz, \tag{6}$$

$$\overline{Q_{\mathrm{loss}}}(x) = \int_{z_s}^{z_t} \rho_d \overline{q_{\mathrm{ten_{neg}}}}(x,z)dz, \tag{7}$$

where ρ_d (unit: kg·m^{-3}) is the air density, $\overline{q_{\mathrm{ten\ pos}}}$ and $\overline{q_{\mathrm{ten\ neg}}}$ (unit: kg·s^{-1}) represent the positive and negative values of the $\overline{q_{\mathrm{ten}}}$, respectively.

2.4.3 The moist Froude number

The Froude number characterizes flow behavior near topography and is defined as:

$$\mathrm{Fr} = \frac{u}{NH_0}, \tag{8}$$

Where u (unit: m·s^{-1}) is the zonal wind speed, H_0 (unit: m) represents the maximum height of topography. N (s^{-1}) denotes the Brunt-Väisälä frequency, which describes the vertical oscillation frequency of an air parcel in a stably stratified atmosphere and serves as a key parameter linking moist convection to terrain-induced dynamical features. It is given by:

$$N = \sqrt{\frac{g}{\theta_v}\left(\frac{d\theta_v}{dz}\right)}, \tag{9}$$

Where θ_v (unit: K) is the virtual potential temperature and g (unit: m·s^{-2}) is the gravity acceleration. It is worth noting that the Brunt-Väisälä frequency should be considered in three stages over the development of moist convection: (1) dry air conditions (original formulation), (2) unsaturated moist air (dry adiabatic processes), and (3) saturated moist air (moist adiabatic processes). The moist Brunt-Väisälä frequency is given by (Durran and Klemp, 1982; Liu and Gao, 2003):

$$N_m = \sqrt{\frac{g}{T}\left(\frac{dT}{dz} + \Gamma_m\right)\left(1 + \frac{Lq_s}{RT}\right) - \frac{g}{1+q_w}\frac{dq_w}{dz}}, \tag{10}$$

Where the pseudo adiabatic lapse rate, Γ_m, is defined as:

https://doi.org/10.5194/egusphere-2026-869
Preprint. Discussion started: 9 April 2026
© Author(s) 2026. CC BY 4.0 License.

$$\Gamma_m = \Gamma_d \frac{(1+q_w)\left(1+\frac{Lq_s}{RT}\right)}{1+\frac{c_{pv}q_s+c_w q_l}{c_p}+\frac{\epsilon L^2 q_s}{c_p RT^2}\left(1+\frac{q_s}{\epsilon}\right)}, \quad (11)$$

In Equations 10 and 11, T (unit: K) is the air temperature, L (unit: J·kg^{-1})is the latent heat of vaporization, q_s (unit: kg·kg^{-1}) is the saturation mixing ratio of water vapor, R (unit: J·kg^{-1}·K^{-1}) is the gas constant for dry air, q_w (unit: kg·kg^{-1}) is the total mixing ratio of water substance, Γ_d (unit: K km^{-1})is the dry-adiabatic lapse rate, c_{pv} (unit: J·kg^{-1}·K^{-1}) is the specific heat capacity of water vapor, c_w (unit: J·kg^{-1}·K^{-1}) is the specific heat capacity of liquid water, q_l (unit: kg·kg^{-1}) is the liquid water mixing ratio, c_p (unit: J·kg^{-1}·K^{-1}) is the specific heat capacity of dry air, and ϵ is the ratio of gas constants for dry air and water vapor. All constants are set to their respective values in the "Constants.F" module of the CM1 source code.

Equations 10 and 11 are based on the warm cloud assumption and account for the thermodynamic effects of water vapor condensation, liquid water, and air-water vapor mixtures. However, clouds over the TP exhibit distinct microphysical properties (Chang et al., 2019; Zhao et al., 2019). Mixed-phase clouds are more prevalent during the warm season over the TP, and the frequency of precipitation is primarily controlled by these clouds (Chang et al., 2019; Wang et al., 2021).

To represent the transition from liquid to ice saturation conditions, a temperature-dependent weighting approach is adopted in mixed-phase clouds. Following standard cloud microphysics practice (Peters et al., 2022; Yau and Rogers, 1996), two reference temperatures were selected: T_0 = 273.15 K (0 °C) and T_i = 233.15 K (−40 °C), which were defined by (Pruppacher and Klett, 2010; Yau and Rogers, 1996). The mixed-phase weighting factor $\alpha(T)$, which represents the fractional contribution of ice, was prescribed as

$$\alpha(T) = \begin{cases} 0, T \geq T_0 \\ \frac{T_0 - T}{T_0 - T_i}, T_i < T < T_0 \\ 1, T \leq T_i \end{cases}, \quad (12)$$

This linear formulation ensures a smooth transition between liquid and ice regimes. Although smoother alternatives exist, the linear weighting has been shown to be effective and computationally efficient (Bolton, 1980; Durran and Klemp, 1982; Emanuel, 1991; Peters et al., 2022).

The weighting was then applied to interpolate between liquid- and ice-based thermodynamic properties. The effective saturation vapor pressure is calculated as

$$e_s^* = (1-\alpha)e_{sw}(T) + \alpha e_{si}(T), \quad (13)$$

where $e_{sw}(T)$ and $e_{si}(T)$ are the saturation vapor pressures over water and ice, respectively. For consistency, the Murphy and Koop (2005) formulations are used to compute these reference values. To ensure physical consistency and numerical stability, supersaturation is prevented in the model by limiting the saturation vapor pressure e_s^* to be less than the ambient pressure. This approach is commonly employed in cloud microphysics models to avoid unphysical supersaturation and to stabilize the numerical solution.

Similarly, the latent heat was interpolated as

$$L_s^* = (1-\alpha)L_v(T) + \alpha L_s(T), \quad (14)$$

https://doi.org/10.5194/egusphere-2026-869
Preprint. Discussion started: 9 April 2026
© Author(s) 2026. CC BY 4.0 License.

where $L_v(T)$ is the latent heat of vaporization and $L_s(T)$ is the latent heat of sublimation.

The corresponding saturation mixing ratio was then obtained as

$$q_s^* = \varepsilon \frac{e_s^*}{p - e_s^*}, \tag{15}$$

Where p denotes the ambient pressure. This formulation ensures that both thermodynamic stability and moist processes are represented consistently across the liquid, mixed-phase, and ice regimes.

$$\Gamma_m = \Gamma_d \frac{(1+q_t)\left(1+\frac{L^* q_s^*}{RT}\right)}{1+\frac{c_{pv} q_s^* + c_w q_l + c_i q_i}{c_p} + \frac{\varepsilon (L^*)^2 q_s^*}{c_p R T^2}\left(1+\frac{q_s^*}{\varepsilon}\right)}, \tag{16}$$

where q_t is the total hydrometeor mixing ratio, q_s^* is the effective saturation mixing ratio, and L_s^* is the mixed-phase latent heat.

$$N_m = \sqrt{\frac{g}{T}\left(\frac{dT}{dz} + \Gamma_m\right)\left(1 + \frac{L^* q_s^*}{RT}\right) - \frac{g}{1+q_t}\frac{dq_t}{dz}}, \tag{17}$$

which incorporates both thermal stratification and the vertical distribution of total water.

Finally, the moist Froude number is given b

$$\mathrm{Fr}_m = \frac{u}{N_m H_0}, \tag{18}$$

The modified moist Froude number Fr_m offers a more accurate representation of convection and stability in moist and mixed-phase atmospheres over the TP. As such, Fr_m is essential for predicting convection initiation, cloud formation, and atmospheric dynamics in lake-mountain regions influenced by moisture.

3. Lake and Topographic effects

3.1 Precipitation distribution

The simulations illustrate the pronounced lake and downstream terrain joint effect on the distribution and intensity of precipitation. Overall, during the whole simulation period, the accumulated precipitation exhibits a characteristic lake-mountain coupled pattern. (Fig. S2). Although largely disorganized, the striated nature of the precipitation pattern suggests weak organization by roll convection. These precipitation features resemble those observed in open-cell lake-effect convection (Sakakibara et al., 1988; Steenburgh and Campbell, 2017; Steiger et al., 2013).

The temporal pattern, quantified by interquartile ranges (25th-75th percentiles), reveals that lake-mountain interactions modulate the timing and variability of precipitation (Fig. 4). The lake-breeze circulation, together with the background flow, causes precipitation to develop preferentially over the lake and supports continued precipitation development beyond the shoreline in experiments involving the lake (Fig. 4). Precipitation appears firstly over the lake (Figs. 4a, b), and subsequently intensifies on the windward and leeward slopes (Figs. 4c-f), and finally shifts farther downstream (Figs. 4g, h), consistent with the direction of background flow. The LM_3000 configuration exhibits an early, mechanically driven precipitation, with peak values occurring within 2-4 h as topographic lifting rapidly enhances condensation and rainfall. However, introducing the lake substantially delays the onset of convection. The initiation of precipitation is postponed until 8-12 h, followed by a sharp and

https://doi.org/10.5194/egusphere-2026-869
Preprint. Discussion started: 9 April 2026
© Author(s) 2026. CC BY 4.0 License.

well-defined peak that is most pronounced over the lake and its downstream region, producing a much steeper temporal gradient in LM_1500. In OL, precipitation peaks even later (approximately 12 h) and is weaker, concentrated mainly over the lake and its downstream area. The LM_750 shares a similar onset time with LM_1500 but yields smaller precipitation amounts. The differences in precipitation are broadly consistent with the relative timescales of thermally driven circulations under clear skies and weak synoptic forcing. Upslope wind can develop early as sloping terrain warms rapidly, promoting mechanically and thermally assisted ascent over the mountain (Barry, 2008; Serafin and Zardi, 2010; Whiteman, 2000). In contrast, lake breeze circulations require a more extended period of daytime heating to establish a sufficient land-water thermal contrast, delaying the initiation of convective activity (Arritt, 1993; Miller et al., 2003). Accordingly, we define the period of strongest overlap between the lake breeze and mountain circulation as the processes of synergistic interaction. Using this definition, we treat times after 7 h as the lake-mountain synergy regime, when cloud and precipitation processes are well developed and begin to influence the downstream.

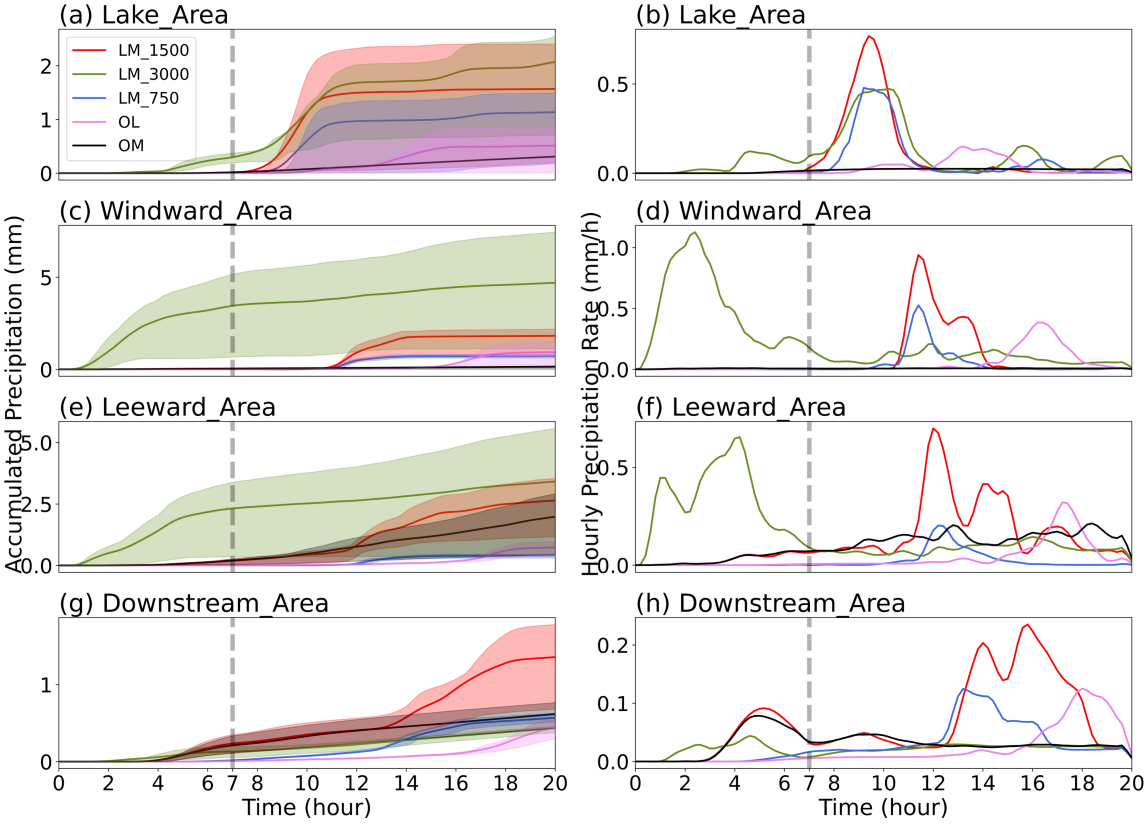


Figure 4. Time series of (left) accumulated precipitation (mm) and (right) hourly precipitation rate (mm h^{-1}) averaged over five subregions: (a-b) Lake Area, (c-d) Windward Area, (e-f) Leeward Area, and (g-h) Downstream Area, for the five experiments: LM_1500, LM_3000, LM_750, OL, and OM. The solid lines denote means, and the shaded envelopes represent the interquartile range (25th-75th percentile) within each configuration.

https://doi.org/10.5194/egusphere-2026-869
Preprint. Discussion started: 9 April 2026
© Author(s) 2026. CC BY 4.0 License.

During the lake-mountain synergy phase, precipitation fields exhibit distinct spatial distributions among the different configurations. In LM_1500, the combination effect of lake-induced moisture and the mechanically forced ascent on the windward slope produce stronger and more concentrated terrain-driven precipitation that extends upslope from the downwind foothills (Fig. 5a). Compared to LM_1500, increasing mountain height shifts the primary rainfall enhancement toward the lake area/windward side and limits precipitation expansion over the leeward, yielding a more confined precipitation footprint on the downstream side (Fig. 5b). By contrast, weaker terrain forcing reduces the vertical ascent, resulting in weaker and more spatially confined precipitation in LM_750 (Fig. 5c). When only the lake is present, precipitation remains largely confined to the lake and its immediate downwind vicinity and is more symmetric about lake-effect rainfall pattern (Fig. 5d). In the absence of the lake, precipitation appears as a narrow in the leeward, terrain-locked band with limited downstream growth, indicating that background moisture is insufficient to sustain broader precipitation (Fig. 5e).

Stronger orographic ascent shifts and amplifies precipitation toward the lake area and the windward slope. In contrast, the lower mountain limits upslope lifting, leading to weaker and more spatially confined rainfall. Removing the mountain enhances precipitation over the lake while suppressing it over the terrain, whereas removing the lake produces a pronounced precipitation deficit over the former lake area and its downwind region. Overall, the combined effects of lake-supplied moisture and terrain ascent govern the intensity, timing, and spatial distribution of precipitation. Removing either component substantially reduces both the spatial coverage and the magnitude of rainfall.

https://doi.org/10.5194/egusphere-2026-869
Preprint. Discussion started: 9 April 2026
© Author(s) 2026. CC BY 4.0 License.

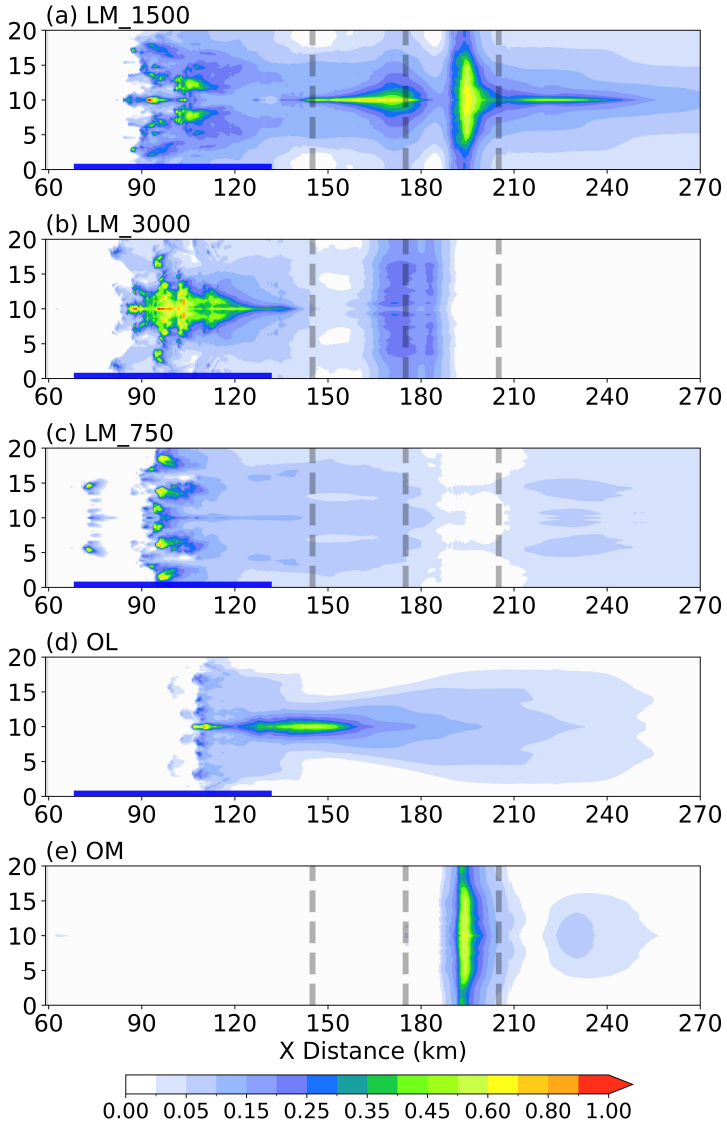


Figure 5. (a) Time-mean precipitation rate (mm h^{-1}) of 13 h in LM_1500. The thick blue line indicates the lake area (x=70-130 km), and the gray dashed lines mark the windward foothill (x=145 km), mountain summit (x=175 km), and leeward foothill (x=205 km). (b), (d), (f), (h) As in (a), but for the LM_3000, LM_750, OL, and OM, respectively. (c) Difference in time-mean precipitation rate (mm h^{-1}) between LM_3000 and LM_1500. (e), (g), (i) As in (c), but showing the differences for LML, OL, and OM relative to ML.

3.2 Moisture and hydrometeor structure

To diagnose the moisture supply, convective instability in a high-altitude environment, we analyze vertical cross sections of water vapor mixing ratio and indicators of convection initiation for the experiments exhibiting distinct precipitation patterns (Fig. 6). In all configurations, near-surface humidity is generally low across the domain, consistent with the dry climatological

https://doi.org/10.5194/egusphere-2026-869
Preprint. Discussion started: 9 April 2026
© Author(s) 2026. CC BY 4.0 License.

background of the TP reported in previous studies (Maussion et al., 2011; You et al., 2015). In the absence of strong external forcing, such a dry environment enhances atmospheric stability, making deep convection difficult to initiate (Fig. S3). This implies that convective initiation is more sensitive to localized moisture enhancements and thermal perturbations. Against this background, surface heterogeneity (lake and adjacent terrain) produces pronounced contrasts in convection initiation.

In LM_1500, LM_3000, and LM_750, lake moistening combined with terrain-forced ascent produces comparatively favorable conditions for convective initiation. Over the lake, a deep moist layer develops between 90 and 150 km, where evaporation increases near-surface humidity and dewpoint, thereby lowering the lifting condensation level (LCL) and the level of free convection (LFC) over the lake relative to the surrounding land (Figs. 6a, c, e). Over the TP, reduced air density often favors a larger kinematic buoyancy flux and a deeper mixed layer, which facilitates vertical moisture transport to support convection initiation (Wang et al., 2020b; Xu et al., 2023). Stronger mixing promotes parcel ascent to the LCL, and subsequent latent heat release helps further into the free convection layer (lower the LCL). Consistent with these changes, CAPE increases and CIN decreases, creating a less inhibited environment for deep convective initiation over the lake areas (Figs. 6b, d, f). Notably, in these simulations, CAPE remains modest even when initiation thresholds are low. Although enhanced moisture supply over the lake lowers the LFC and weakens CIN, CAPE accumulation is still constrained by the thermodynamic background of the TP. Convection may initiate under relatively weak inhibition, but sustained deep development is less favorable than in warm and moist plains. In lowland environments, numerous studies have shown that substantial CAPE can accumulate beneath a strong capping inversion and be released quickly once the cap is breached (Chen et al., 2020a; Emanuel, 2023). Where the LCL-LFC separation remains large, parcels are less likely to reach free convection without additional lifting, implying a greater dependence on windward moisture advection and terrain-forced lifting around 150 km. It should be noted that as mountain height increases, CAPE over the lake region increases and CIN weakens (Figs. 6b, d, f), whereas precipitation over the lake exhibits the opposite tendency (Figs. 5a-c).

In OL, the lake enhances low-level moisture directly, lowering LCL and LFC over the water surface (Figs. 6g-h). However, the absence of orographic lifting inhibits forcing ascent. Although CAPE is elevated over the lake, CIN remains substantial downwind (near 150 km) and the LFC stays relatively high, indicating suppressed convective development away from the lake. In OM, the near-surface layer is drier and the LFC is higher (Figs. 6i-j). CAPE is weak to nearly absent across much of the section, while CIN remains strong. Although terrain-forced ascent occurs near the crest, the conditions remain unfavorable for deep, sustained convection. On the leeward slope (around 180 km), CAPE decreases while CIN increases, indicating a more stable lee environment. Rolling ascent associated with trapped lee waves may nevertheless locally erode inhibition and support the development of convection and produce rain shadow regions (Bai et al., 2021; Zängl, 2005), consistent with the precipitation signal on the leeward slope (Figs. 5a, e). Over the TP, lake moistening alone favors lower LCL but provides limited triggering, whereas terrain forcing without lake moisture yields strong inhibition and weak instability. The interplay between lake-sourced moisture and the downstream orography is critical for modulating convective initiation.

https://doi.org/10.5194/egusphere-2026-869
Preprint. Discussion started: 9 April 2026
© Author(s) 2026. CC BY 4.0 License.

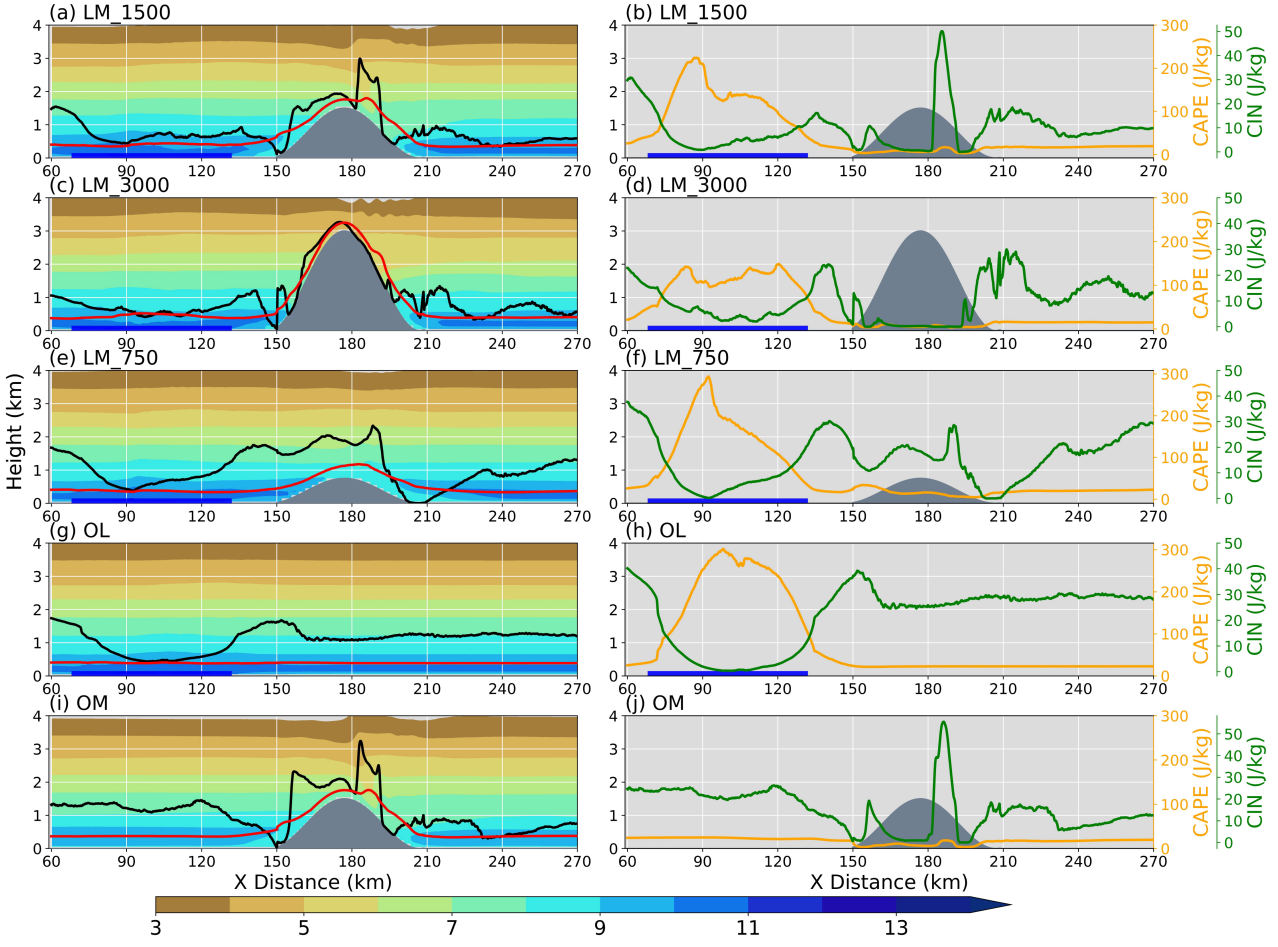


Figure 6. (a-b) Vertical cross sections of the 7-20 h time-mean, 15-km *y*-averaged (over the central domain) water vapor mixing ratio (shading, g kg^{-1}) in the LM_1500. The left panels (a) show the lifted condensation level (LCL; red lines) and the level of free convection (LFC; black lines). The right panels (b) show the surface-based convective available potential energy (CAPE; orange lines, right axis) and convective inhibition (CIN; green lines, left axis) along the cross section. (c-d), (e-f), (g-h), (i-j) As in (a-b), but for the LM_3000, LM_750, OL, and OM, respectively. The thick blue line represents the lake surface, and the gray shading represents the terrain height (m).

Having established the thermodynamic preconditions for initiation, we next examine convective growth and cloud formation using the hydrometeor fields (Fig. 7). The LM_1500 exhibits the deepest convective development, with an enhanced total water column extending above 4 km and collocated with the strongest updraft core (Fig. 7a). Hydrometeors are mainly concentrated near and above the LCL, indicating that near-surface layer water vapor supplied by the lake plays a key role in promoting condensation (Fig. 6a). Notably, the isentropes (θ) rise sharply and fold over the mountain crest, indicating strong diabatic heating within the convective column. When topographic lifting is present, vertical motions reach sufficient magnitude and depth to overcome CIN and support deep convective updrafts capable of initiating precipitation (Figs. 7a-c, f).

https://doi.org/10.5194/egusphere-2026-869
Preprint. Discussion started: 9 April 2026
© Author(s) 2026. CC BY 4.0 License.

Contrasts among configurations clarify the distinct roles of moisture supply and dynamical triggering. With the lake retained and a higher mountain in LM_3000, ascent intensifies over the windward slope, producing more hydrometeors, but the condensate column is narrower and less laterally extensive than in LM_1500 (Fig. 7b). Consistent with the thermodynamic differences diagnosed in the previous section, CAPE over the lake sector is reduced as mountain height increases, and condensate loading over the lake correspondingly decreases, whereas condensate becomes more concentrated near the crest where orographic ascent is strongest. With a lower mountain (LM_750), cloud development is shallower and hydrometeor is reduced (Fig. 7c), consistent with weaker mechanical forcing that makes it more difficult to reach the LFC. In OL, low-level moistening together with the lake-land thermal contrast forcing generates a broad and shallow convective response (Fig. 7e). Although relatively strong vertical motion develops over the lake, the absence of terrain-forced lifting limits further convective development. In contrast, hydrometeor in OM is only caused by the lee wave, indicating strong moisture limitation in the absence of lake, with convection development supported only by the background flow (Fig. 7f). Overall, these configurations indicate that deep convection occurs when moisture supports with suitable orographic lifting, promoting efficient condensation and sustained vertical development.

https://doi.org/10.5194/egusphere-2026-869
Preprint. Discussion started: 9 April 2026
© Author(s) 2026. CC BY 4.0 License.

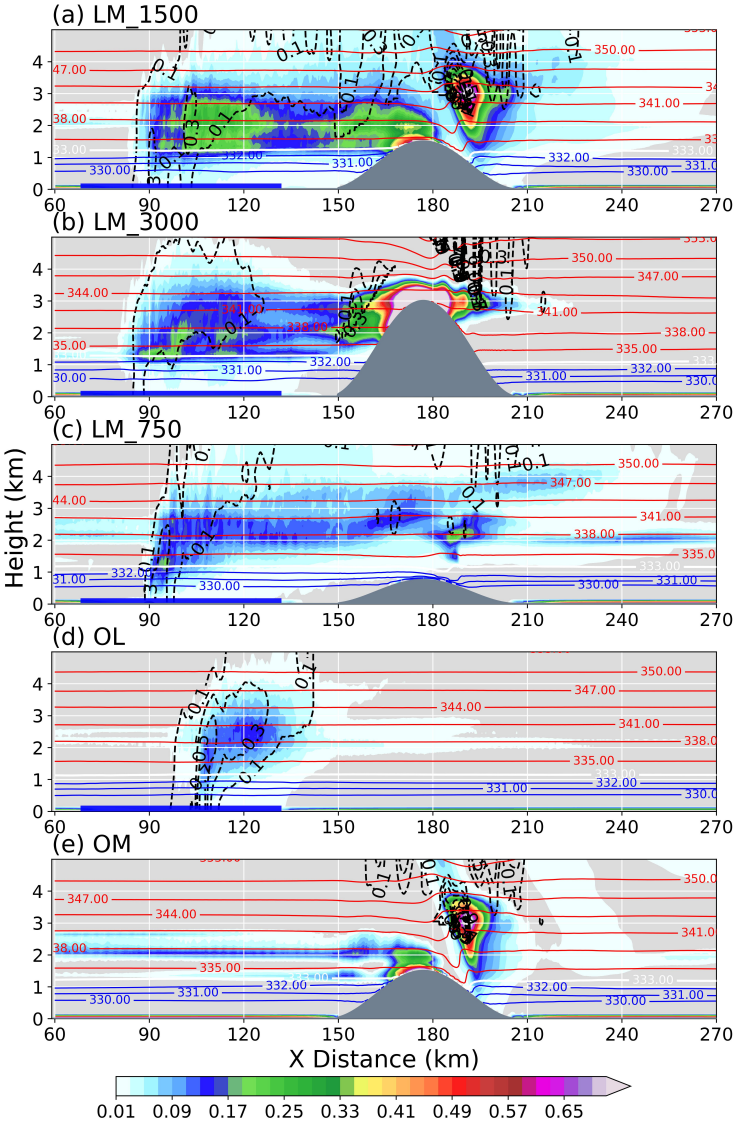


Figure 7. (a) Vertical cross sections of the 7-20 h time-mean, 15-km *y*-averaged (over the central domain) total hydrometeor mixing ratio (shading, g kg^{-1}) in the LM_1500. The potential temperature (blue-to-red contour lines, K) and vertical velocity (black dashed contour lines, only plotted positive values, m s^{-1}). The vertical velocity field is smoothed with a 20 × 20-point uniform filter. Panel (b), (c), (d) and (e), same as panel (a), but for the LM_3000, LM_750, OL, and OM, respectively. The thick blue line represents the lake surface, and the gray shading represents the terrain height (m).

3.3. Hydrometeor tendency and condensate

To further characterize the evolution of convective growth and condensate production, we examine the temporal evolution of the vertical profiles of total non-rain hydrometeor content ($q_{hc} = q_c + q_i + q_s + q_g$) and rain water mixing ratio q_r, averaged over

https://doi.org/10.5194/egusphere-2026-869
Preprint. Discussion started: 9 April 2026
© Author(s) 2026. CC BY 4.0 License.

the lake, mountain, and downstream subregions (Fig. 8). Across the involving lake configurations, low-level moisture promotes early hydrometeor formation over the lake, but the subsequent vertical deepening and conversion to rainwater vary markedly. The q_{hc} occur primarily above the freezing level (1.4-1.5 km; not shown), indicating that cloud condensate mass accumulates through efficient ice-phase growth (e.g., riming and aggregation) within the mixed-phase layer. As these hydrometeors descend through the freezing level, melting increases q_r, so rainwater maxima occur mainly below the freezing level. This vertical structure suggests that precipitation is primarily produced through ice-crystal processes of precipitation, with hydrometeors growing aloft and melting as they fall through the melting layer, rather than through warm-rain processes (Gupta et al., 2023). In LM_1500, hydrometeor content develops rapidly over the lake, and q_r increases sharply between 8-12 h (Fig. 8a). Over the mountain, the hydrometeor column is deeper and more persistent (Fig. 8b). Trapped lee waves promote enhanced production of q_{hc} aloft and a more efficient conversion to q_r. The downstream response subsequently strengthens (16 h; Fig. 8c), consistent with the timing of precipitation shown in Fig. 4b. In LM_3000, hydrometeor growth and rainwater production begin earlier, but the lake-region hydrometeor column is narrower and less vertically developed (Fig. 8d), consistent with stronger inhibition (higher LFC and larger CIN) limiting deepening. Over the mountain, both q_{hc} and q_r maximize at low levels, producing intense orographically forced precipitation (Fig. 8f). In LM_750, reduced terrain height weakens lifting; q_{hc} increases over both the lake and mountain, but q_r remains comparatively weak (Figs. 8g-i). In OL, hydrometeors persist over the lake and its downwind region for most of the simulation period, with their evolution lagging behind that in the other configurations (Figs. 8j-l). Lake-breeze forcing is able to maintain cloudiness, but in the absence of strong dynamical lifting it is inefficient at rapidly converting condensate into q_r. Both q_{hc} and q_r remain low across all subregions (Figs. 8m-o), indicating that moisture limitation is pronounced in OM.

Downstream hydrometeor amounts are generally lower than those over the lake and mountain in all configurations, and the downstream precipitation signal primarily reflects the evolution of upstream systems rather than strong local production. Overall, earlier and stronger rainfall occurs when lake moistening coincides with terrain-induced lifting, consistent with the precipitation evolution shown in Fig. 4.

https://doi.org/10.5194/egusphere-2026-869
Preprint. Discussion started: 9 April 2026
© Author(s) 2026. CC BY 4.0 License.

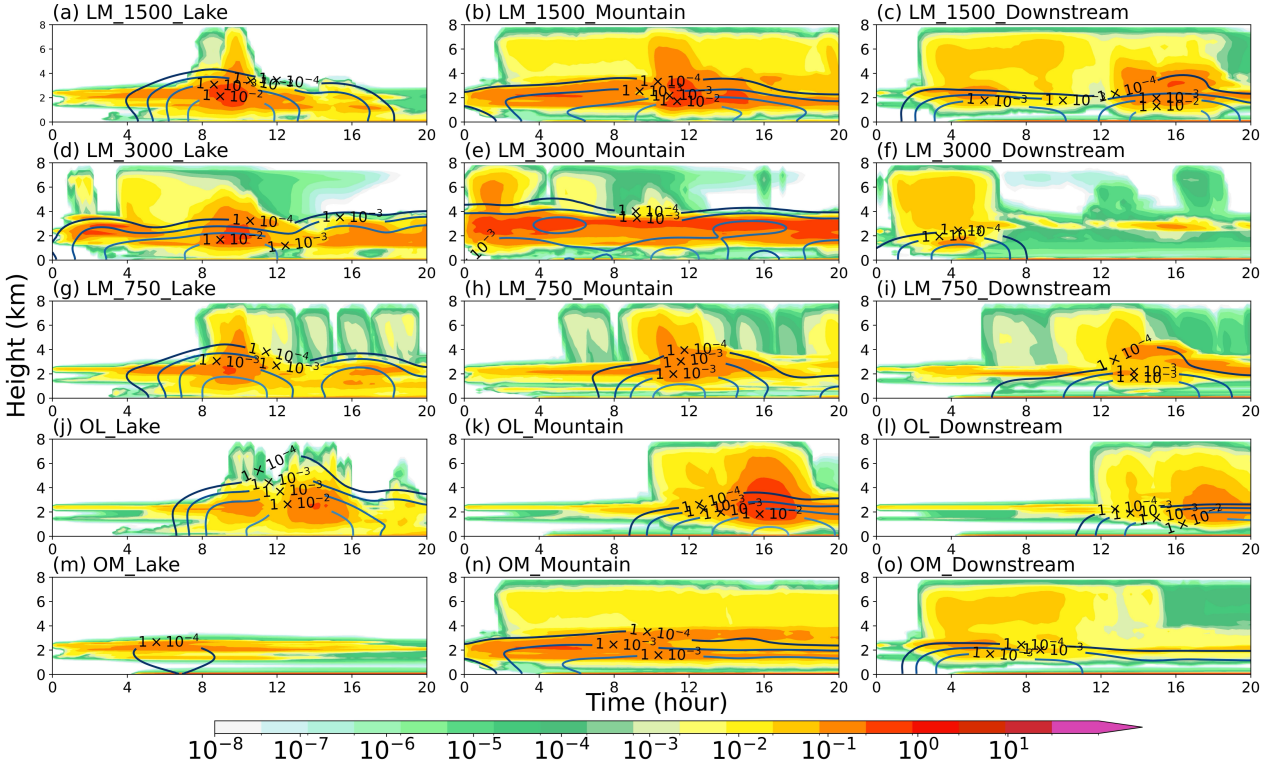


Figure 8. Temporal evolution of the 15-km *y*-averaged (over the central domain) cloud condensate mixing ratios in. Colored shading shows the total cloud condensate $q_{hc} = q_c + q_i + q_s + q_g$ (including cloud water, cloud ice, snow, and graupel; g kg^{-1}), and contour lines denote the rainwater mixing ratio q_r (g kg^{-1}), both averaged over the (left) lake, (middle) mountain, and (right) downstream subregions. Panels (a-c) correspond to LM_1500, (d-f) to LM_3000, (g-i) to LM_750, (j-l) to OL, and (m-o) to OM.

To diagnose how lake-terrain forcing regulates condensate production and its conversion to surface precipitation over the TP, Figure 9 shows the distributions of hydrometeor mass growth (Q_{growth}), hydrometeor mass loss (Q_{loss}), and the surface precipitation mass rate (P_r).

Across all lake-present experiments, the first Q_{growth} peak occurs on the downwind side of the lake area (80-110 km), further proving the near-surface moistening promote convection initiation (Fig. 9a). In the same sector, the Q_{loss} and P_r also exhibit peak (Figs. 9b-c), indicating efficient conversion of hydrometeors to precipitation. Only LM_1500 and LM_3000 exhibit a second, stronger paired maximum of Q_{growth} and Q_{loss} in the windward slope (145-175 km), collocated with a peak in P_r. However, in LM_750 and OL, the absence or weakness of terrain-induced lifting results in the precipitation formation is inhabited. Along the leeward slope, the configurations with the same mountain height (LM_1500 and OM) exhibit pronounced differences in Q_{growth} and Q_{loss}, but their maximum P_r are comparable. This indicates that forced ascent associated with trapped lee wave can substantially enhance precipitation release even under limited moisture.

Over the TP, the distinctive thermodynamic background constrains the magnitude and distribution of hydrometeor and finally shapes the precipitation pattern (Fu et al., 2020; Xu et al., 2023). In previous studies over the plains using an open water

https://doi.org/10.5194/egusphere-2026-869
Preprint. Discussion started: 9 April 2026
© Author(s) 2026. CC BY 4.0 License.

configuration comparable to OM, Q_{growth} and P_r typically exceed Q_{loss} by about one order of magnitude (Gowan et al., 2021), reflecting the more moist near-surface layer and lower saturation deficit. In contrast, over the TP, Q_{growth}, Q_{loss}, and P_r are of comparable magnitude and all smaller than the plains, indicating the condensate budget that is limited by moisture and convection initiation. Specifically, the low moisture condition and elevated lifting condensation levels over the TP, together with stronger entrainment of dry air, limit condensate production, thereby delaying saturation and suppressing the development of deep convection (Li et al., 2022a; Wang et al., 2020b). As a result, even under comparable dynamical forcing, Q_{growth} increases more slowly than over the plains. Notably, despite the weaker Q_{growth}, the efficiency of converting condensate into P_r does not decrease with altitude. Mixed-phase processes are prevalent over the TP (as shown in Fig. 8), and ice-phase growth processes can efficiently generate precipitation (Gao et al., 2018). These processes partly compensate for the relatively low Q_{growth} and high Q_{loss}, yielding P_r comparable to that over the plains. In this setting, convective clouds tend to be short-lived and spatially limited, with frequent precipitation occurrence but typically weaker event intensity, consistent with the constrained moisture supply and inhibited deep maintenance over the TP (Chen et al., 2019; Fu et al., 2020; Singh and Nakamura, 2009; Ueno et al., 2007).

https://doi.org/10.5194/egusphere-2026-869
Preprint. Discussion started: 9 April 2026
© Author(s) 2026. CC BY 4.0 License.

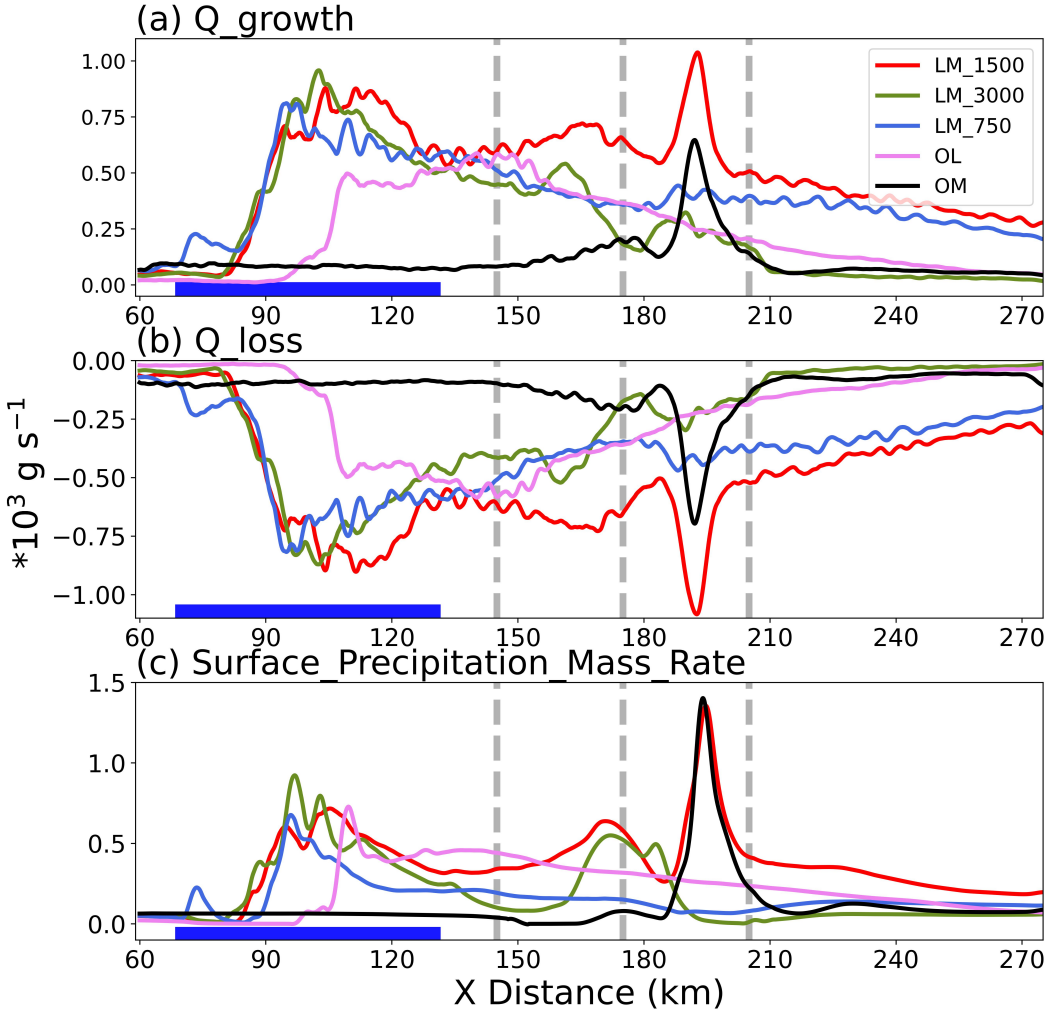


Figure 9. Zonal distributions of the 7-20 h time-mean, 15-km *y*-averaged (over the central domain) of (a) hydrometeor mass growth rate (10^2 kg s^{-1}), (b) hydrometeor mass loss rate (10^2 kg s^{-1}), and (c) surface precipitation mass rate (10^2 kg s^{-1}) for the four experiments. The thick blue line indicates the lake area (*x*=70-130 km), and the gray dashed lines mark the windward foothill (*x*=145 km), mountain summit (*x*=175 km), and leeward foothill (*x*=205 km).

3.4 Thermodynamic mechanism and Moisture supply pathways

To further assess convective triggering under different surface configurations, Fig. 10 illustrates vertical cross-sections of potential temperature perturbation (θ') and wind perturbation. These fields highlight localized circulation and thermodynamic anomalies and are used to relate dynamical forcing to the corresponding cloud development.

In LM_1500, the upstream of the mountain (60-150 km) exhibits a clear vertical contrast in θ' (Fig. 10a). Near the windward foot, terrain blocking promotes low-level cold-air pooling and a thicker stable layer, yielding negative θ' within low-level layer.

https://doi.org/10.5194/egusphere-2026-869
Preprint. Discussion started: 9 April 2026
© Author(s) 2026. CC BY 4.0 License.

Above this layer, positive θ' develops as convection over the lake intensifies, consistent with diabatic warming associated with sustained condensation and deposition. At the same time, a deep ascending branch is collocated with the windward slope and extends above 6 km. Above the mountain, a cold core ($\theta' < -0.5$ K) associated with lifted isentropes is collocated with the condensate region (Fig. 7a), indicating that ascent and adiabatic cooling over the leeward support hydrometeor of condensate growth and transport to the downstream. In LM_3000, stronger orographic lifting leads to larger cold and warm θ' perturbations above the mountain, collocated with enhanced hydrometeor and precipitation (Figs. 7b and 5b). At the same time, subsidence warming on the lee slope is more pronounced, effectively cutting off the low-level moisture pathway. As a result, more residual hydrometeors are recirculated back over the lake region and melt into precipitation (Fig. 8d), which weakens the warm potential temperature anomaly aloft over the lake. In LM_750, θ′ is weaker and ascent is shallower, consistent with a lower and more diffuse hydrometeor distribution (Fig. 7c).

Vertical transport is shallow over the lake, with weak θ′ confined below 3-4 km in OL (Fig. 10d). The absence of sharp vertical motion or strong θ′ limits the development of deep convective clouds. The shallow hydrometeors are transported to the downstream driven by the background flow (Fig. 7d). In OM, the intense windward updraft and strong warm core are evident above the mountain, yet hydrometeor remains limited in extent (Fig. 7e), indicating that strong lifting cannot sustain the development of deep convection cloud under moisture-limited conditions. Overall, the synergy between low-level instability supplied by the lake and terrain lifting favors the initiation and development of deep convection.

https://doi.org/10.5194/egusphere-2026-869
Preprint. Discussion started: 9 April 2026
© Author(s) 2026. CC BY 4.0 License.

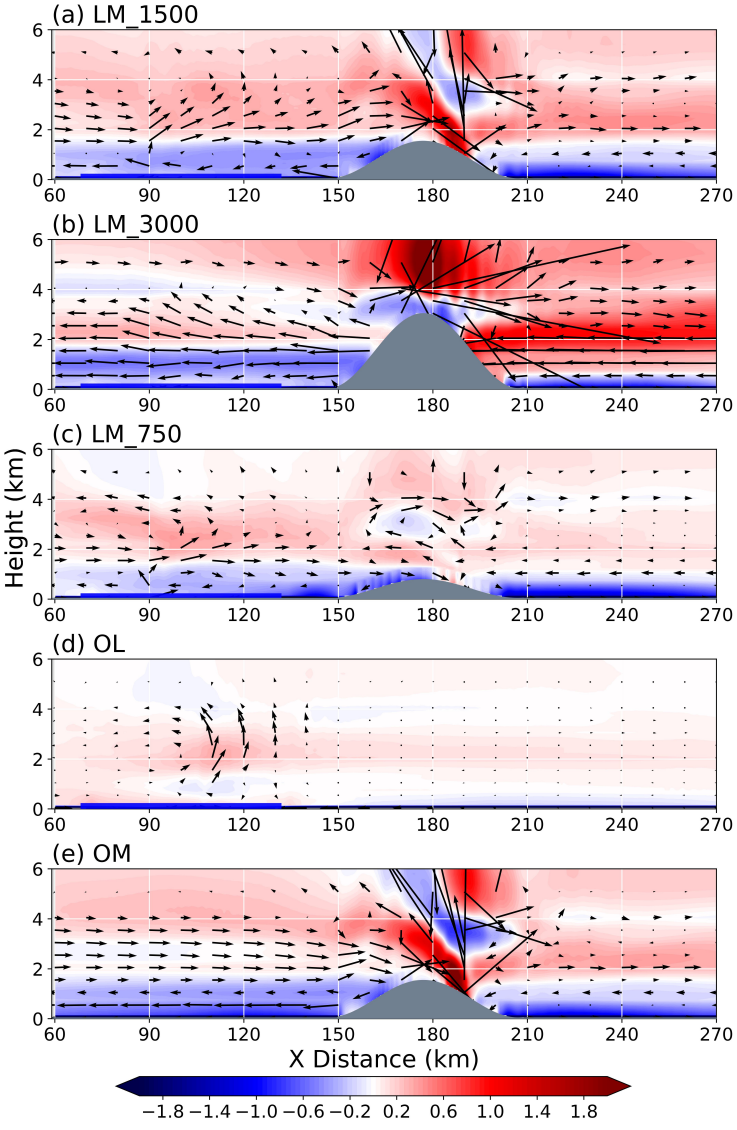


Figure 10. (a) Vertical cross sections of the 7-20 h time-mean, 15-km *y*-averaged (over the central domain) perturbation potential temperature (shading, θ', K) in the LM_1500. The cross-section-parallel wind vectors composed by the perturbation zonal wind (u') and vertical velocity (w). The wind-vector field is smoothed with a 20 × 20-point uniform filter. (b), (c), (d) and (e) As in (a), but for the LM_3000, LM_750, OL, and OM experiments, respectively. The thick blue line represents the lake surface, and the gray shading represents the terrain height (m).

To connect the dynamic structure diagnosed in the different configurations with the downstream evolution of clouds and precipitation, we further quantify the moist dynamical regime using the moist Froude number (Fr_m) (Fig. 11). For relatively small upstream values of Fr_m, the background flow is blocked by the topographic barrier, collected with the perturbation zonal

https://doi.org/10.5194/egusphere-2026-869
Preprint. Discussion started: 9 April 2026
© Author(s) 2026. CC BY 4.0 License.

wind at low level (Fig. 10). When the lake is set in experiments, the moisture supply leads to lower N_m. and further strengthen the Fr_m.

In LM_1500, the strongest and most vertically extensive upstream Fr_m anomalies indicate that the combined lake and terrain act to weaken moist stability and to enhance the dynamical lifting (Fig. 11a). This pattern supports the development of convection and sustained hydrometeor production. However, increasing the terrain height cause dynamical competition (Fig. 11b). While the stronger mechanical lifting provides more kinetic energy to overcome the potential energy of the topographic barrier, the larger H in Fr_m exhibits more blocked effect near the mountain. This moist dynamic response tends to concentrate convection and precipitation on the mountain while promoting the downstream drying tendency. In LM_750 (Fig. 11c), the near-surface moisture persists, but the lifting is weaker and less vertically extended. Accordingly, this configuration is less effective at transporting low-level moisture to the development of deep convection compared with the LM_1500. In OL, Fr_m only serves as a compact diagnostic of U/N_m, the near-surface moisture reduces effective moist stability and promotes shallow lifting even in the absence of mechanical forcing (Fig. 11d). In OM, where the low-level moisture supply is absent, convective initiation is restricted and the development of deep convection is suppressed despite favorable orographic lifting (Fig. 11e).

https://doi.org/10.5194/egusphere-2026-869
Preprint. Discussion started: 9 April 2026
© Author(s) 2026. CC BY 4.0 License.

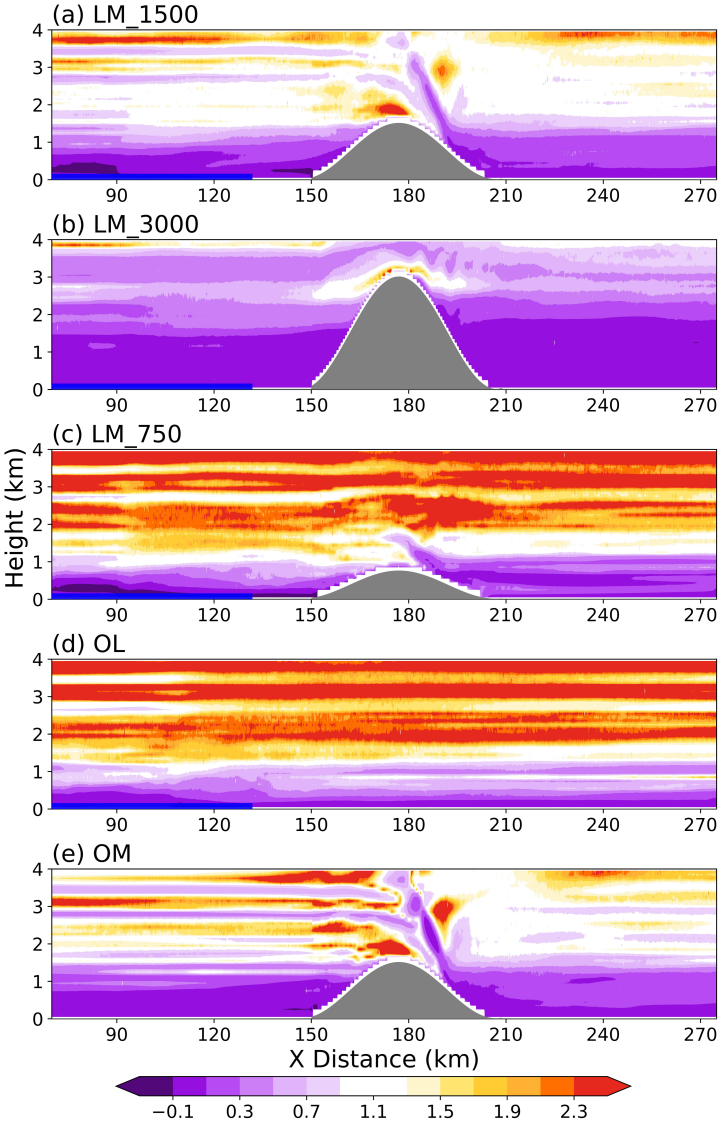


Figure 11. (a) Vertical cross sections of the 7-20 h time-mean, 15-km *y*-averaged most Froude number in the LM_1500. (b), (c), (d) and (e) As in (a), but for the LM_3000, LM_750, OL, and OM, respectively. The thick blue line represents the lake surface, and the gray shading represents the terrain height (m).

To diagnose how lake-terrain forcing regulates the pathways by which near-surface moisture supply affects convection, Fig. 12 shows forward trajectories of tracer particles released in the upstream near-surface (z=50 m, x=80 km) for the different configurations. Forward trajectories were computed from the model output using an open-source Python package developed by (Gowan, 2019)). Although water vapor can generate phase changes, our purpose is not to construct a closed moisture budget, but rather to diagnose the transport pathways and lifting of near-surface moisture from the lake toward the terrain and

https://doi.org/10.5194/egusphere-2026-869
Preprint. Discussion started: 9 April 2026
© Author(s) 2026. CC BY 4.0 License.

downstream, thereby isolating the thermodynamic and dynamical linkages between moisture transport and orographic triggering for convective development.

In LM_1500, lake-supplied tracer parcels lift and spread laterally to the downstream under the background flow (Fig. 12a). Terrain forcing organizes a coherent upslope ascent branch along the windward slope (Fig. 12b), transporting moisture from the mountain foot to levels more favorable for cloud growth and precipitation formation. On the leeward slope, the trapped lee wave produces two downstream branches: one pathway is lifted by the ascending phase of the lee wave and advected downstream aloft, while the other follows the descending phase and channels moisture downstream within the lower levels. In LM_3000, stronger orographic lifting causes more moisture to be retained near the mountain front rather than transported farther downstream (Figs. 12c-d). Trajectories released closer to the terrain also show a clearer blocking for the higher mountain (Fig. S4). Compared with LM_1500 and LM_3000, LM_750 still exhibits moisture transport, but only shallow lifting occurs, and fewer trajectories reach higher levels (Figs. 12e-f). In OL, a moist tongue develops over the lake and its downwind areas. most trajectories remain within this humid zone and are transported primarily horizontally with modest lateral spreading (Fig. 12g). Vertical transport is weak, with trajectories largely confined to low levels and lacking sustained deep ascent (Fig. 12h). In OM, trajectories show a narrow ascent near the terrain, but moisture content is lower than in the involving lake experiments.

https://doi.org/10.5194/egusphere-2026-869
Preprint. Discussion started: 9 April 2026
© Author(s) 2026. CC BY 4.0 License.

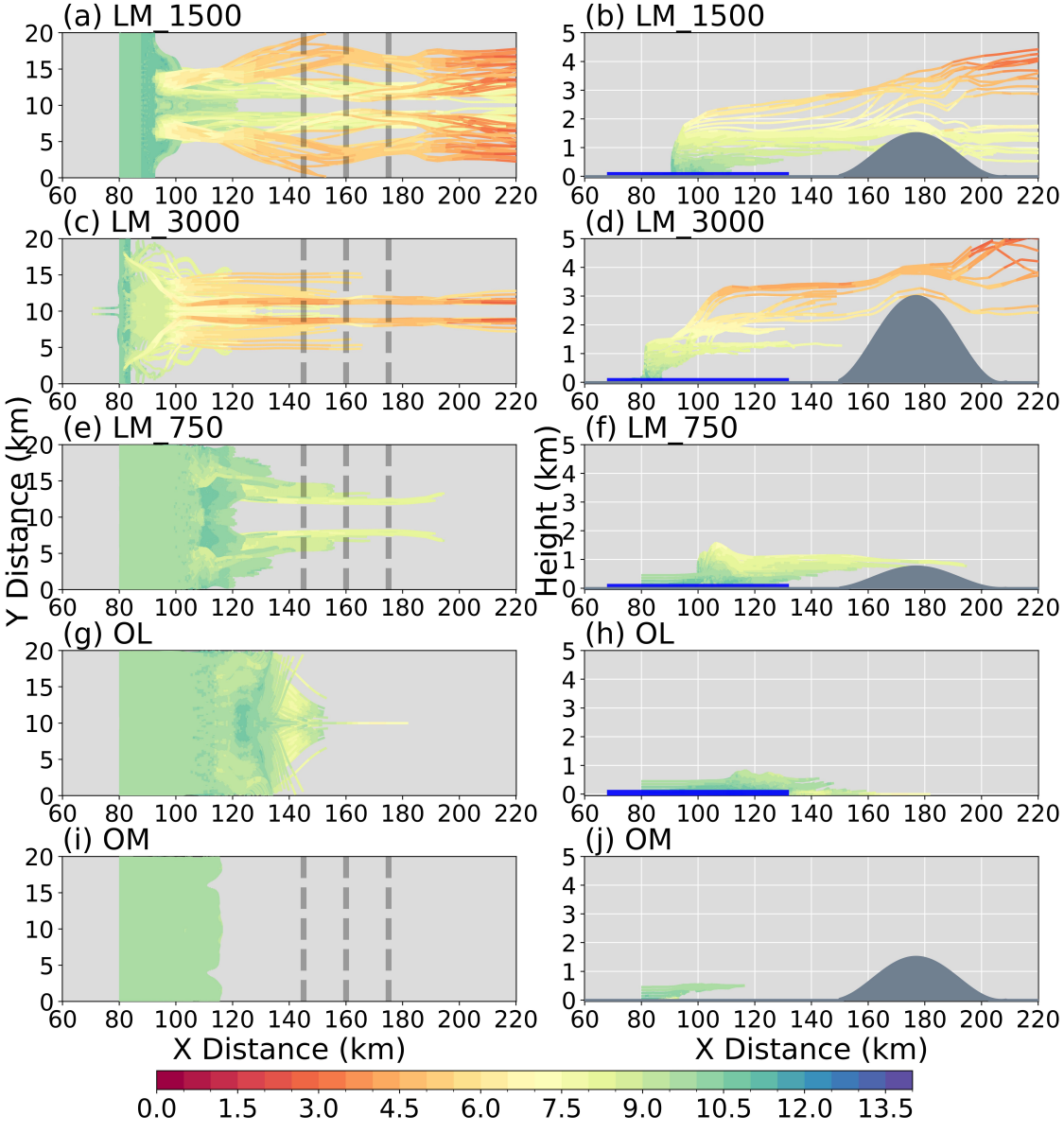


Figure 12. Forward trajectories of water vapor (g kg^{-1}) tracer particles released at x = 80 km and z = 50 m in experiments with lake presence, including (a) LM_1500, (b) LM_3000, (c) LM_750, (d) OL and (e) OM. The left column shows particle trajectories projected onto the x-y plane, while the right column presents trajectories in the x-z plane.

https://doi.org/10.5194/egusphere-2026-869
Preprint. Discussion started: 9 April 2026
© Author(s) 2026. CC BY 4.0 License.

4. Conclusions and Discussion

Using idealized large-eddy simulations with Cloud Model 1 (CM1), we isolate how the lake and downstream topography with prescribed heights jointly regulate clouds and precipitation over the Tibetan Plateau (TP) under weak synoptic forcing. Specifically, the mountain height is treated as a control parameter for configurations involving both lake and mountain, along with lake-only, mountain-only, and no heterogeneity reference experiments. Deep convection over the TP is strongly constrained by convective initiation in the high-elevation environment with scarce moisture. Lake-driven moistening provides thermodynamic support by increasing low-level humidity and weakening inhibition. Orographic lifting promotes the further development of deep convection, while variations in mountain height lead to competing lifting and blocking effects that modulate local and downstream cloud and precipitation responses.

The lake-mountain coupling promotes convective development and enhances precipitation formation when both lake moisture supply and mountain lifting are present. This coupling is particularly important over the TP, where convection is highly sensitive to its initial conditions. Lake evaporation increases low-level humidity and lowers LCL/LFC while reducing CIN over the lake. These changes lower the barrier to convective triggering in an atmosphere that is otherwise prone to limited moist support. However, lake forcing alone produces only a shallow, weakly precipitating response, because lake-breeze convergence provides limited deep ascent and the background TP environment inhibits sustained vertical growth. However, lake forcing alone produces only a shallow, weakly precipitating response, because the lake-breeze effect provides limited deep ascent and the background TP environment inhibits sustained vertical growth. In contrast, in the absence of the lake, mechanically forced ascent occurs over the mountain, but precipitation remains confined to a narrow area near the mountain because the moisture supply is limited. The strongest and most extensive precipitation occurs when lake-supplied moisture is lifted over the downstream mountain. Despite reduced condensate production under limited moisture availability, strong terrain lifting enhances the efficiency of converting condensate into TP precipitation through ice-phase processes.

Downstream mountain height modulates the competition between orographic lifting and blocking in the presence of lake-supplied moisture. This modulation is particularly important over the TP, where moisture and energy are limited and convective development depends strongly on the efficiency with which low-level moisture is transported into the free convection layer. As mountain height increases, stronger orographic ascent concentrates precipitation on the upstream side of the mountain. At the same time, enhanced blocking limits low-level moisture transport and suppresses downstream convective development. Conversely, lower mountain retains the lake-induced moistening and permits moisture transport over a broader horizontal extent. However, weaker orographic lifting provides less vertical development, making sustained deep convective growth more difficult. Overall, the lake provides thermodynamic support by enhancing low-level moisture and lowering the threshold for convective initiation. In contrast, the mountain combines lifting with blocking to modulate convective development and reshape the spatial distribution and downstream extent of precipitation.

Although the idealized simulation enables clean mechanistic attribution, several limitations should be considered. First, the alpine open lake and bell-shaped mountain suppress realistic shoreline, geometry, and subgrid-scale topography. Over the TP,

https://doi.org/10.5194/egusphere-2026-869
Preprint. Discussion started: 9 April 2026
© Author(s) 2026. CC BY 4.0 License.

the position and persistence of convection are readily influenced by complex terrain and land-surface heterogeneity (Ma et al., 2008; Wu et al., 2023; Yang et al., 2025). Second, this study employs a single thermodynamic profile and a background wind representative of weak synoptic forcing, so the conclusions are most applicable to TP where convective initiation is a primary constraint. Given the limited moisture over the TP and the strong modulation of low-level circulation by thermally driven topographic flows, the coupled response may differ under different background moisture and stability, or under stronger large-scale forcing. Finally, hydrometeor partitioning and precipitation efficiency depend on microphysical assumptions (Korolev et al., 2017). Over the TP, frequent mixed-phase processes and limited moisture availability increase the relative importance of ice-phase processes, amplifying microphysical uncertainties.

This study targets TP environments where convective initiation is a primary constraint, with the aim of elucidating the synergy between lake and mountain. We note that mountain gravity wave propagation, modulated by mountain height and width, associated with leeward dynamical processes (Frame and Markowski, 2006; Xu et al., 2017; Xue et al., 2022), may further influence downstream cloud and precipitation processes. Future work will therefore pursue a more systematic dynamical diagnosis and mechanistic assessment of these pathways.

Data availability. Data used in this paper can be provided upon request from Jinghua Chen (jhchen@nuist.edu.cn) or Tianliang Zhao (tlzhao@nuist.edu.cn).

Author contributions. KY: Data curation, Methodology, Investigation, Writing - original draft. JC, TZ, XX, CL and SF: Conceptualization, Methodology, Writing - review & editing. JC and TZ: Conceptualization, Methodology. YL, QY, ZL, ZL, LW, and YJ: Investigation, Conceptualization. All authors commented on the paper.

Competing interests. The authors declare that they have no conflict of interest.

Acknowledgement. This research was supported by the Xinjiang Talent Development Foundation (XJRC-2025-ZZB-ZDXQ-018), the National Key Research and Development Program of China (No. 2023YFC3007504), the National Science Foundation of China (42075067), the Jiangsu Graduate Student Research Innovation Program (KYCX25_1605, KYCX25_1617).

https://doi.org/10.5194/egusphere-2026-869
Preprint. Discussion started: 9 April 2026
© Author(s) 2026. CC BY 4.0 License.

References

Arritt, R. W.: Effects of the large-scale flow on characteristic features of the sea breeze, J. Appl. Meteor., 32, 116–125, https://doi.org/10.1175/1520-0450(1993)032<0116:EOTLSF>2.0.CO;2, 1993.

Bai, L., Chen, G., Huang, Y., and Meng, Z.: Convection Initiation at a Coastal Rainfall Hotspot in South China: Synoptic Patterns and Orographic Effects, JGR Atmospheres, 126, e2021JD034642, https://doi.org/10.1029/2021JD034642, 2021.

Barros, A. P., Joshi, M., Putkonen, J., and Burbank, D. W.: A study of the 1999 monsoon rainfall in a mountainous region in central nepal using TRMM products and rain gauge observations, Geophysical Research Letters, 27, 3683–3686, https://doi.org/10.1029/2000GL011827, 2000.

Barry, R. G.: Mountain weather and climate third edition, 3rd ed., Cambridge University Press, Cambridge, https://doi.org/10.1017/CBO9780511754753, 2008.

Biggs, W. G. and Graves, M. E.: A lake breeze index, J. Appl. Meteor., 1, 474–480, https://doi.org/10.1175/1520-0450(1962)001<0474:ALBI>2.0.CO;2, 1962.

Bolton, D.: The computation of equivalent potential temperature, Mon. Wea. Rev., 108, 1046–1053, https://doi.org/10.1175/1520-0493(1980)108<1046:TCOEPT>2.0.CO;2, 1980.

Bryan, G. H. and Fritsch, J. M.: A Benchmark Simulation for Moist Nonhydrostatic Numerical Models, Mon. Wea. Rev., 130, 2917–2928, https://doi.org/10.1175/1520-0493(2002)130<2917:ABSFMN>2.0.CO;2, 2002.

Chang, Y., Guo, X., Tang, J., and Lu, G.: Aircraft measurement campaign on summer cloud microphysical properties over the tibetan plateau, Sci Rep, 9, 4912, https://doi.org/10.1038/s41598-019-41514-5, 2019.

Chen, F. and Avissar, R.: The Impact of Land-Surface Wetness Heterogeneity on Mesoscale Heat Fluxes, J. Appl. Meteor., 33, 1323–1340, https://doi.org/10.1175/1520-0450(1994)033<1323:TIOLSW>2.0.CO;2, 1994.

Chen, J., Wu, X., Yin, Y., Huang, Q., and Xiao, H.: Characteristics of Cloud Systems over the Tibetan Plateau and East China during Boreal Summer, J. Climate, 30, 3117–3137, https://doi.org/10.1175/JCLI-D-16-0169.1, 2017.

Chen, J., Wu, X., Yin, Y., Lu, C., Xiao, H., Huang, Q., and Deng, L.: Thermal Effects of the Surface Heat Flux on Cloud Systems over the Tibetan Plateau in Boreal Summer, Journal of Climate, 32, 4699–4714, https://doi.org/10.1175/JCLI-D-18-0604.1, 2019.

Chen, J., Dai, A., Zhang, Y., and Rasmussen, K. L.: Changes in convective available potential energy and convective inhibition under global warming, Journal of Climate, 33, 2025–2050, https://doi.org/10.1175/JCLI-D-19-0461.1, 2020a.

Chen, J., Hagos, S., Xiao, H., Fast, J. D., and Feng, Z.: Characterization of Surface Heterogeneity-Induced Convection Using Cluster Analysis, JGR Atmospheres, 125, https://doi.org/10.1029/2020jd032550, 2020b.

Chen, J., Wu, X., Yin, Y., and Lu, C.: Large-Scale Circulation Environment and Microphysical Characteristics of the Cloud Systems Over the Tibetan Plateau in Boreal Summer, Earth and Space Science, 7, e2020EA001154, https://doi.org/10.1029/2020EA001154, 2020c.

https://doi.org/10.5194/egusphere-2026-869
Preprint. Discussion started: 9 April 2026
© Author(s) 2026. CC BY 4.0 License.

Chen, Y., Zhang, A., Chen, S., Tu, C., Li, W., and Fu, Y.: Enhancement of ice-phase precipitation caused by thermal forcing produces ghost echoes over the Tibetan Plateau, npj Clim Atmos Sci, 4, 41, https://doi.org/10.1038/s41612-021-00199-2, 2021.

Deardorff, J. W.: Stratocumulus-capped mixed layers derived from a three-dimensional model, Boundary-Layer Meteorol, 18, 495–527, https://doi.org/10.1007/BF00119502, 1980.

Dehghan, A., Mariani, Z., Leroyer, S., Sills, D., Bélair, S., and Joe, P.: Evaluation of Modeled Lake Breezes Using an Enhanced Observational Network in Southern Ontario: Case Studies, Journal of Applied Meteorology and Climatology, 57, 1511–1534, https://doi.org/10.1175/JAMC-D-17-0231.1, 2018.

Durran, D. R. and Klemp, J. B.: On the effects of moisture on the brunt-väisälä frequency, J. Atmos. Sci., 39, 2152–2158, https://doi.org/10.1175/1520-0469(1982)039<2152:OTEOMO>2.0.CO;2, 1982.

Emanuel, K.: On the physics of high CAPE, Journal of the Atmospheric Sciences, 80, 2669–2683, https://doi.org/10.1175/JAS-D-23-0060.1, 2023.

Emanuel, K. A.: A scheme for representing cumulus convection in large-scale models, J. Atmos. Sci., 48, 2313–2329, https://doi.org/10.1175/1520-0469(1991)048<2313:ASFRCC>2.0.CO;2, 1991.

Estoque, M. A., Gross, J., and Lai, H. W.: A Lake Breeze over Southern Lake Ontario, Mon. Wea. Rev., 104, 386–396, https://doi.org/10.1175/1520-0493(1976)104<0386:ALBOSL>2.0.CO;2, 1976.

Feldmann, M., Rotunno, R., Germann, U., and Berne, A.: Supercell Thunderstorms in Complex Topography—How Mountain Valleys with Lakes Can Increase Occurrence Frequency, Monthly Weather Review, 152, 471–489, https://doi.org/10.1175/MWR-D-22-0350.1, 2024.

Frame, J. and Markowski, P.: The interaction of simulated squall lines with idealized mountain ridges, Monthly Weather Review, 134, 1919–1941, https://doi.org/10.1175/MWR3157.1, 2006.

Frye, J. D. and Mote, T. L.: Convection Initiation along Soil Moisture Boundaries in the Southern Great Plains, Monthly Weather Review, 138, 1140–1151, https://doi.org/10.1175/2009MWR2865.1, 2010.

Fu, Y., Liu, G., Wu, G., Yu, R., Xu, Y., Wang, Y., Li, R., and Liu, Q.: Tower mast of precipitation over the central Tibetan Plateau summer, Geophysical Research Letters, 33, 2005GL024713, https://doi.org/10.1029/2005GL024713, 2006.

Fu, Y., Ma, Y., Zhong, L., Yang, Y., Guo, X., Wang, C., Xu, X., Yang, K., Xu, X., Liu, L., Fan, G., Li, Y., and Wang, D.: Land-surface processes and summer-cloud-precipitation characteristics in the Tibetan Plateau and their effects on downstream weather: a review and perspective, National Science Review, 7, 500–515, https://doi.org/10.1093/nsr/nwz226, 2020.

Gao, W., Liu, L., Li, J., and Lu, C.: The Microphysical Properties of Convective Precipitation Over the Tibetan Plateau by a Subkilometer Resolution Cloud-Resolving Simulation, JGR Atmospheres, 123, 3212–3227, https://doi.org/10.1002/2017JD027812, 2018.

Gowan, T. M.: Trajectories (personal GitHub page), 2019.

Gowan, T. M., Steenburgh, W. J., and Minder, J. R.: Downstream Evolution and Coastal-to-Inland Transition of Landfalling Lake-Effect Systems, Monthly Weather Review, 149, 1023–1040, https://doi.org/10.1175/MWR-D-20-0253.1, 2021.

https://doi.org/10.5194/egusphere-2026-869
Preprint. Discussion started: 9 April 2026
© Author(s) 2026. CC BY 4.0 License.

Gowan, T. M., Steenburgh, W. J., and Minder, J. R.: Orographic Effects on Landfalling Lake-Effect Systems, Monthly Weather Review, 150, 2013–2031, https://doi.org/10.1175/MWR-D-21-0314.1, 2022.

Gupta, A. K., Deshmukh, A., Waman, D., Patade, S., Jadav, A., Phillips, V. T. J., Bansemer, A., Martins, J. A., and Gonçalves, F. L. T.: The microphysics of the warm-rain and ice crystal processes of precipitation in simulated continental convective storms, Commun Earth Environ, 4, 226, https://doi.org/10.1038/s43247-023-00884-5, 2023.

Haeberli, W., Buetler, M., Huggel, C., Friedli, T. L., Schaub, Y., and Schleiss, A. J.: New lakes in deglaciating high-mountain regions – opportunities and risks, Climatic Change, 139, 201–214, https://doi.org/10.1007/s10584-016-1771-5, 2016.

Henderson-Sellers, B.: Calculating the surface energy balance for lake and reservoir modeling: A review, Reviews of Geophysics, 24, 625–649, https://doi.org/10.1029/RG024i003p00625, 1986.

Hu, L., Deng, D., Gao, S., and Xu, X.: The seasonal variation of Tibetan Convective Systems: Satellite observation, JGR Atmospheres, 121, 5512–5525, https://doi.org/10.1002/2015JD024390, 2016.

Huss, M. and Hock, R.: Global-scale hydrological response to future glacier mass loss, Nature Clim Change, 8, 135–140, https://doi.org/10.1038/s41558-017-0049-x, 2018.

Immerzeel, W. W., Van Beek, L. P. H., and Bierkens, M. F. P.: Climate Change Will Affect the Asian Water Towers, Science, 328, 1382–1385, https://doi.org/10.1126/science.1183188, 2010.

Jiang, G.-S. and Shu, C.-W.: Efficient Implementation of Weighted ENO Schemes, Journal of Computational Physics, 126, 202–228, https://doi.org/10.1006/jcph.1996.0130, 1996.

Jiménez, P. A., Dudhia, J., González-Rouco, J. F., Navarro, J., Montávez, J. P., and García-Bustamante, E.: A Revised Scheme for the WRF Surface Layer Formulation, Monthly Weather Review, 140, 898–918, https://doi.org/10.1175/MWR-D-11-00056.1, 2012.

Kalthoff, N., Adler, B., Barthlott, Ch., Corsmeier, U., Mobbs, S., Crewell, S., Träumner, K., Kottmeier, Ch., Wieser, A., Smith, V., and Di Girolamo, P.: The impact of convergence zones on the initiation of deep convection: A case study from COPS, Atmospheric Research, 93, 680–694, https://doi.org/10.1016/j.atmosres.2009.02.010, 2009.

Kang, S., Xu, Y., You, Q., Flügel, W.-A., Pepin, N., and Yao, T.: Review of climate and cryospheric change in the Tibetan Plateau, Environ. Res. Lett., 5, 015101, https://doi.org/10.1088/1748-9326/5/1/015101, 2010.

Katona, B. and Markowski, P.: Assessing the Influence of Complex Terrain on Severe Convective Environments in Northeastern Alabama, Weather and Forecasting, 36, 1003–1029, https://doi.org/10.1175/WAF-D-20-0136.1, 2021.

Keen, C. S. and Lyons, W. A.: Lake/land breeze circulations on the western shore of lake michigan, J. Appl. Meteor., 17, 1843–1855, https://doi.org/10.1175/1520-0450(1978)017<1843:LBCOTW>2.0.CO;2, 1978.

Khodayar Pardo, S.: High-resolution analysis of the initiation of deep convection forced by boundary-layer processes, KIT Scientific Publishing, 2015.

Klemp, J. B. and Wilhelmson, R. B.: The Simulation of Three-Dimensional Convective Storm Dynamics, J. Atmos. Sci., 35, 1070–1096, https://doi.org/10.1175/1520-0469(1978)035<1070:TSOTDC>2.0.CO;2, 1978.

https://doi.org/10.5194/egusphere-2026-869
Preprint. Discussion started: 9 April 2026
© Author(s) 2026. CC BY 4.0 License.

Korolev, A., McFarquhar, G., Field, P. R., Franklin, C., Lawson, P., Wang, Z., Williams, E., Abel, S. J., Axisa, D., Borrmann, S., Crosier, J., Fugal, J., Krämer, M., Lohmann, U., Schlenczek, O., Schnaiter, M., and Wendisch, M.: Mixed-Phase Clouds: Progress and Challenges, Meteorological Monographs, 58, 5.1-5.50, https://doi.org/10.1175/AMSMONOGRAPHS-D-17-0001.1, 2017.

Kristovich, D. A. R. and Steve, R. A.: A Satellite Study of Cloud-Band Frequencies over the Great Lakes, J. Appl. Meteor., 34, 2083–2090, https://doi.org/10.1175/1520-0450(1995)034<2083:ASSOCB>2.0.CO;2, 1995.

Kristovich, D. A. R., Clark, R. D., Frame, J., Geerts, B., Knupp, K. R., Kosiba, K. A., Laird, N. F., Metz, N. D., Minder, J. R., Sikora, T. D., Steenburgh, W. J., Steiger, S. M., Wurman, J., and Young, G. S.: The ontario winter lake-effect systems field campaign: Scientific and educational adventures to further our knowledge and prediction of lake-effect storms, Bulletin of the American Meteorological Society, 98, 315–332, https://doi.org/10.1175/BAMS-D-15-00034.1, 2017.

Laird, N. F., Kristovich, D. A. R., and Walsh, J. E.: Idealized Model Simulations Examining the Mesoscale Structure of Winter Lake-Effect Circulations, Mon. Wea. Rev., 131, 206–221, https://doi.org/10.1175/1520-0493(2003)131<0206:IMSETM>2.0.CO;2, 2003.

Lee, J. M., Zhang, Y., and Klein, S. A.: The Effect of Land Surface Heterogeneity and Background Wind on Shallow Cumulus Clouds and the Transition to Deeper Convection, Journal of the Atmospheric Sciences, 76, 401–419, https://doi.org/10.1175/JAS-D-18-0196.1, 2019.

Li, C., Zuo, Q., Xu, X., and Gao, S.: Water vapor transport around the Tibetan Plateau and its effect on summer rainfall over the Yangtze River valley, J Meteorol Res, 30, 472–482, https://doi.org/10.1007/s13351-016-5123-1, 2016.

Li, J., Yue, Z., Lu, C., Chen, J., Wu, X., Xu, X., Luo, S., Zhu, L., Wu, S., Wang, F., and He, X.: Convective Entrainment Rate over the Tibetan Plateau and Its Adjacent Regions in the Boreal Summer Using SNPP-VIIRS, Remote Sensing, 14, 2073, https://doi.org/10.3390/rs14092073, 2022a.

Li, X., Long, D., Scanlon, B. R., Mann, M. E., Li, X., Tian, F., Sun, Z., and Wang, G.: Climate change threatens terrestrial water storage over the Tibetan Plateau, Nat. Clim. Chang., 12, 801–807, https://doi.org/10.1038/s41558-022-01443-0, 2022b.

Linsbauer, A., Frey, H., Haeberli, W., Machguth, H., Azam, M. F., and Allen, S.: Modelling glacier-bed overdeepenings and possible future lakes for the glaciers in the himalaya—karakoram region, Ann. Glaciol., 57, 119–130, https://doi.org/10.3189/2016AoG71A627, 2016.

Liu, D. and Gao, S.: THE BRUNT-VAISALA FREQUENCY IN A SATURATED ATMOSPHERE AND THE REVISED EQUIVALENT POTENTIAL TEMPERATURE., Acta Meteorologica Sinica, (3), 379–383, https://doi.org/10.11676/qxxb2003.037, 2003.

Liu, Y., Bao, Q., Duan, A., Qian, Z., and Wu, G.: Recent progress in the impact of the Tibetan Plateau on climate in China, Adv. Atmos. Sci., 24, 1060–1076, https://doi.org/10.1007/s00376-007-1060-3, 2007.

Luo, Y., Zhang, R., Qian, W., Luo, Z., and Hu, X.: Intercomparison of Deep Convection over the Tibetan Plateau–Asian Monsoon Region and Subtropical North America in Boreal Summer Using CloudSat/CALIPSO Data, Journal of Climate, 24, 2164–2177, https://doi.org/10.1175/2010JCLI4032.1, 2011.

https://doi.org/10.5194/egusphere-2026-869
Preprint. Discussion started: 9 April 2026
© Author(s) 2026. CC BY 4.0 License.

Lyons, W. A.: The climatology and prediction of the chicago lake breeze, J. Appl. Meteor., 11, 1259–1270, https://doi.org/10.1175/1520-0450(1972)011<1259:TCAPOT>2.0.CO;2, 1972.

Lyons, W. A. and Cole, H. S.: Fumigation and plume trapping on the shores of lake michigan during stable onshore flow, J. Appl. Meteor., 12, 494–510, https://doi.org/10.1175/1520-0450(1973)012<0494:FAPTOT>2.0.CO;2, 1973.

Ma, Y., Menenti, M., Feddes, R., and Wang, J.: Analysis of the land surface heterogeneity and its impact on atmospheric variables and the aerodynamic and thermodynamic roughness lengths, J. Geophys. Res., 113, 2007JD009124, https://doi.org/10.1029/2007JD009124, 2008.

Maussion, F., Scherer, D., Finkelnburg, R., Richters, J., Yang, W., and Yao, T.: WRF simulation of a precipitation event over the Tibetan Plateau, China – an assessment using remote sensing and ground observations, Hydrol. Earth Syst. Sci., 15, 1795–1817, https://doi.org/10.5194/hess-15-1795-2011, 2011.

McGowan, H. A., Owens, I. F., and Sturman, A. P.: Thermal and dynamic characteristics of alpine lake breezes, lake tekapo, new zealand, Boundary-Layer Meteorol, 76, 3–24, https://doi.org/10.1007/BF00710888, 1995.

Miller, S. T. K., Keim, B. D., Talbot, R. W., and Mao, H.: Sea breeze: Structure, forecasting, and impacts, Reviews of Geophysics, 41, 2003RG000124, https://doi.org/10.1029/2003RG000124, 2003.

Morrison, H., Curry, J. A., and Khvorostyanov, V. I.: A New Double-Moment Microphysics Parameterization for Application in Cloud and Climate Models. Part I: Description, Journal of the Atmospheric Sciences, 62, 1665–1677, https://doi.org/10.1175/JAS3446.1, 2005.

Murphy, D. M. and Koop, T.: Review of the vapour pressures of ice and supercooled water for atmospheric applications, Quarterly Journal of the Royal Meteorological Society: A journal of the atmospheric sciences, applied meteorology and physical oceanography, 131, 1539–1565, 2005.

Peace, R. L. and Sykes, R. B.: Mesoscale study of a lake effect snow storm, Mon. Wea. Rev., 94, 495–507, https://doi.org/10.1175/1520-0493(1966)094<0495:MSOALE>2.3.CO;2, 1966.

Peters, J. M., Mulholland, J. P., and Chavas, D. R.: Generalized lapse rate formulas for use in entraining CAPE calculations, Journal of the Atmospheric Sciences, 79, 815–836, https://doi.org/10.1175/JAS-D-21-0118.1, 2022.

Pruppacher, H. and Klett, J.: Microphysics of clouds and precipitation. Springer, 2010.

Qie, X., Wu, X., Yuan, T., Bian, J., and Lu, D.: Comprehensive Pattern of Deep Convective Systems over the Tibetan Plateau–South Asian Monsoon Region Based on TRMM Data, Journal of Climate, 27, 6612–6626, https://doi.org/10.1175/JCLI-D-14-00076.1, 2014.

Qiu, J.: China: The third pole, Nature, 454, 393–396, https://doi.org/10.1038/454393a, 2008.

Rieck, M., Hohenegger, C., and Van Heerwaarden, C. C.: The Influence of Land Surface Heterogeneities on Cloud Size Development, Monthly Weather Review, 142, 3830–3846, https://doi.org/10.1175/MWR-D-13-00354.1, 2014.

Rotunno, R., Klemp, J. B., and Weisman, M. L.: A theory for strong, long-lived squall lines, J. Atmos. Sci., 45, 463–485, https://doi.org/10.1175/1520-0469(1988)045<0463:ATFSLL>2.0.CO;2, 1988.

https://doi.org/10.5194/egusphere-2026-869
Preprint. Discussion started: 9 April 2026
© Author(s) 2026. CC BY 4.0 License.

Rousseau-Rizzi, R., Kirshbaum, D. J., and Yau, M. K.: Initiation of Deep Convection over an Idealized Mesoscale Convergence Line, Journal of the Atmospheric Sciences, 74, 835–853, https://doi.org/10.1175/JAS-D-16-0221.1, 2017.

Rüthrich, F., Reudenbach, C., Thies, B., and Bendix, J.: Lake-Related Cloud Dynamics on the Tibetan Plateau: Spatial Patterns and Interannual Variability, Journal of Climate, 28, 9080–9104, https://doi.org/10.1175/JCLI-D-14-00698.1, 2015.

Sakakibara, H., Ishihara, M., and Yanagisawa, Z.: Classification of mesoscale snowfall systems observed in western hokuriku during a heavy snowfall period in january 1984, Journal of the Meteorological Society of Japan, 66, 193–199, https://doi.org/10.2151/jmsj1965.66.1_193, 1988.

Serafin, S. and Zardi, D.: Daytime heat transfer processes related to slope flows and turbulent convection in an idealized mountain valley, Journal of the Atmospheric Sciences, 67, 3739–3756, https://doi.org/10.1175/2010JAS3428.1, 2010.

Sills, D. M. L., Brook, J. R., Levy, I., Makar, P. A., Zhang, J., and Taylor, P. A.: Lake breezes in the southern Great Lakes region and their influence during BAQS-Met 2007, Atmos. Chem. Phys., 11, 7955–7973, https://doi.org/10.5194/acp-11-7955-2011, 2011.

Singh, P. and Nakamura, K.: Diurnal variation in summer precipitation over the central Tibetan Plateau, J. Geophys. Res., 114, 2009JD011788, https://doi.org/10.1029/2009JD011788, 2009.

Steenburgh, W. J. and Campbell, L. S.: The OWLeS IOP2b lake-effect snowstorm: Shoreline geometry and the mesoscale forcing of precipitation, Mon. Wea. Rev., 145, 2421–2436, https://doi.org/10.1175/MWR-D-16-0460.1, 2017.

Steiger, S. M., Schrom, R., Stamm, A., Ruth, D., Jaszka, K., Kress, T., Rathbun, B., Frame, J., Wurman, J., and Kosiba, K.: Circulations, bounded weak echo regions, and horizontal vortices observed within long-lake-axis-parallel–lake-effect storms by the doppler on wheels*, Monthly Weather Review, 141, 2821–2840, https://doi.org/10.1175/MWR-D-12-00226.1, 2013.

Su, D., Wen, L., Gao, X., Leppäranta, M., Song, X., Shi, Q., and Kirillin, G.: Effects of the Largest Lake of the Tibetan Plateau on the Regional Climate, JGR Atmospheres, 125, e2020JD033396, https://doi.org/10.1029/2020JD033396, 2020.

Sulla-Menashe, D. and Friedl, M. A.: User guide to collection 6 MODIS land cover (MCD12Q1 and MCD12C1) product, Usgs: Reston, Va, Usa, 1, 18, 2018.

Ueno, K., Tanaka, K., Tsutsui, H., and Li, M.: Snow Cover Conditions in the Tibetan Plateau Observed during the Winter of 2003/2004, Arctic, Antarctic, and Alpine Research, 39, 152–164, https://doi.org/10.1657/1523-0430(2007)39[152:SCCITT]2.0.CO;2, 2007.

Wang, B., Ma, Y., Ma, W., Su, B., and Dong, X.: Evaluation of ten methods for estimating evaporation in a small high-elevation lake on the Tibetan Plateau, Theor Appl Climatol, 136, 1033–1045, https://doi.org/10.1007/s00704-018-2539-9, 2019.

Wang, J., Huang, L., Ju, J., Daut, G., Ma, Q., Zhu, L., Haberzettl, T., Baade, J., Mäusbacher, R., Hamilton, A., Graves, K., Olsthoorn, J., and Laval, B. E.: Seasonal stratification of a deep, high-altitude, dimictic lake: Nam Co, Tibetan Plateau, Journal of Hydrology, 584, 124668, https://doi.org/10.1016/j.jhydrol.2020.124668, 2020a.

https://doi.org/10.5194/egusphere-2026-869
Preprint. Discussion started: 9 April 2026
© Author(s) 2026. CC BY 4.0 License.

Wang, J., Jian, B., Wang, G., Zhao, Y., Li, Y., Letu, H., Zhang, M., and Li, J.: Climatology of cloud phase, cloud radiative effects and precipitation properties over the tibetan plateau, Remote Sensing, 13, 363, https://doi.org/10.3390/rs13030363, 2021.

Wang, Y., Zeng, X., Xu, X., Welty, J., Lenschow, D. H., Zhou, M., and Zhao, Y.: Why Are There More Summer Afternoon Low Clouds Over the Tibetan Plateau Compared to Eastern China?, Geophysical Research Letters, 47, e2020GL089665, https://doi.org/10.1029/2020GL089665, 2020b.

Warren, R. A., Kirshbaum, D. J., Plant, R. S., and Lean, H. W.: A 'Boscastle-type' quasi-stationary convective system over the UK Southwest Peninsula, Quart J Royal Meteoro Soc, 140, 240–257, https://doi.org/10.1002/qj.2124, 2014.

Whiteman, C. D.: Mountain meteorology: Fundamentals and applications, Oxford University Press, https://doi.org/10.1093/oso/9780195132717.001.0001, 2000.

Wilhelmson, R. B. and Chen, C.-S.: A Simulation of the Development of Successive Cells Along a Cold Outflow Boundary, J. Atmos. Sci., 39, 1466–1483, https://doi.org/10.1175/1520-0469(1982)039<1466:ASOTDO>2.0.CO;2, 1982.

Wood, R., Stromberg, I. M., and Jonas, P. R.: Aircraft observations of sea-breeze frontal structure, Quart J Royal Meteoro Soc, 125, 1959–1995, https://doi.org/10.1002/qj.49712555804, 1999.

Wu, G., Duan, A., Liu, Y., Mao, J., Ren, R., Bao, Q., He, B., Liu, B., and Hu, W.: Tibetan Plateau climate dynamics: recent research progress and outlook, National Science Review, 2, 100–116, https://doi.org/10.1093/nsr/nwu045, 2015.

Wu, G., Zhou, X., Xu, X., Huang, J., Duan, A., Yang, S., Hu, W., Ma, Y., Liu, Y., Bian, J., Fu, Y., Yang, H., Zhao, P., Zhong, L., and Ma, W.: An Integrated Research Plan for the Tibetan Plateau Land–Air Coupled System and Its Impacts on the Global Climate, Bulletin of the American Meteorological Society, 104, E158–E177, https://doi.org/10.1175/BAMS-D-21-0293.1, 2023.

Wu, Y., Huang, A., Yang, B., Dong, G., Wen, L., Lazhu, Zhang, Z., Fu, Z., Zhu, X., Zhang, X., and Cai, S.: Numerical study on the climatic effect of the lake clusters over Tibetan Plateau in summer, Clim Dyn, 53, 5215–5236, https://doi.org/10.1007/s00382-019-04856-4, 2019.

Xiao, H., Berg, L. K., and Huang, M.: The Impact of Surface Heterogeneities and Land-Atmosphere Interactions on Shallow Clouds Over ARM SGP Site, J Adv Model Earth Syst, 10, 1220–1244, https://doi.org/10.1029/2018ms001286, 2018.

Xu, L., Liu, H., Du, Q., Liu, Y., Sun, J., Xu, A., and Meng, X.: Characteristics of Lake Breezes and Their Impacts on Energy and Carbon Fluxes in Mountainous Areas, Adv. Atmos. Sci., 38, 603–614, https://doi.org/10.1007/s00376-020-0298-x, 2021.

Xu, X., Zhou, M., Chen, J., Bian, L., Zhang, G., Liu, H., Li, S., Zhang, H., Zhao, Y., Suolongduoji, and Jizhi, W.: A comprehensive physical pattern of land-air dynamic and thermal structure on the Qinghai-Xizang Plateau, Sci. China Ser. D-Earth Sci., 45, 577–594, https://doi.org/10.1360/02yd9060, 2002.

Xu, X., Lu, C., Shi, X., and Gao, S.: World water tower: An atmospheric perspective, Geophysical Research Letters, 35, 2008GL035867, https://doi.org/10.1029/2008GL035867, 2008.

Xu, X., Shu, S., and Wang, Y.: Another look on the structure of mountain waves: A spectral perspective, Atmospheric Research, 191, 156–163, https://doi.org/10.1016/j.atmosres.2017.03.015, 2017.

https://doi.org/10.5194/egusphere-2026-869
Preprint. Discussion started: 9 April 2026
© Author(s) 2026. CC BY 4.0 License.

Xu, X., Tang, Y., Wang, Y., Zhang, H., Liu, R., and Zhou, M.: Triggering effects of large topography and boundary layer turbulence on convection over the Tibetan Plateau, Atmos. Chem. Phys., 23, 3299–3309, https://doi.org/10.5194/acp-23-3299-2023, 2023.

Xue, H. and Giorgetta, M. A.: A Large-Eddy Simulation Study on the Diurnally Evolving Nonlinear Trapped Lee Waves over a Two-Dimensional Steep Mountain, Journal of the Atmospheric Sciences, 78, 399–415, https://doi.org/10.1175/JAS-D-20-0085.1, 2021.

Xue, H., Giorgetta, M. A., and Guo, J.: The daytime trapped lee wave pattern and evolution induced by two small-scale mountains of different heights, Quart J Royal Meteoro Soc, 148, 1300–1318, https://doi.org/10.1002/qj.4262, 2022.

Yang, K., Koike, T., Fujii, H., Tamura, T., Xu, X., Bian, L., and Zhou, M.: The Daytime Evolution of the Atmospheric Boundary Layer and Convection over the Tibetan Plateau: Observations and Simulations, Journal of the Meteorological Society of Japan, 82, 1777–1792, https://doi.org/10.2151/jmsj.82.1777, 2004.

Yang, K., Ye, B., Zhou, D., Wu, B., Foken, T., Qin, J., and Zhou, Z.: Response of hydrological cycle to recent climate changes in the Tibetan Plateau, Climatic Change, 109, 517–534, https://doi.org/10.1007/s10584-011-0099-4, 2011.

Yang, K., Chen, J., Wu, X., Yin, Y., Zhao, T., Lu, C., Deng, L., and Ding, H.: Effects of the Indian summer monsoon on the cloud characteristics over the Eastern Tibetan Plateau: a simulation study, Clim Dyn, https://doi.org/10.1007/s00382-024-07219-w, 2024.

Yang, K., Chen, J., Zhao, T., Lu, C., Xu, X., Luo, Y., Yang, Q., Tan, C., Fu, W., and Wang, Z.: Effects of fine terrain complexity on cloud and precipitation changes over the Tibetan Plateau: a modeling study, npj Clim Atmos Sci, 8, 22, https://doi.org/10.1038/s41612-025-00907-2, 2025.

Yao, T., Thompson, L., Yang, W., Yu, W., Gao, Y., Guo, X., Yang, X., Duan, K., Zhao, H., Xu, B., Pu, J., Lu, A., Xiang, Y., Kattel, D. B., and Joswiak, D.: Different glacier status with atmospheric circulations in Tibetan Plateau and surroundings, Nature Clim Change, 2, 663–667, https://doi.org/10.1038/nclimate1580, 2012.

Yao, T., Bolch, T., Chen, D., Gao, J., Immerzeel, W., Piao, S., Su, F., Thompson, L., Wada, Y., Wang, L., Wang, T., Wu, G., Xu, B., Yang, W., Zhang, G., and Zhao, P.: The imbalance of the Asian water tower, Nat Rev Earth Environ, 3, 618–632, https://doi.org/10.1038/s43017-022-00299-4, 2022.

Yao, X., Yang, K., Zhou, X., Wang, Y., Lazhu, Chen, Y., and Lu, H.: Surface friction contrast between water body and land enhances precipitation downwind of a large lake in Tibet, Clim Dyn, 56, 2113–2126, https://doi.org/10.1007/s00382-020-05575-x, 2021.

Yao, X., Yang, K., Letu, H., Zhou, X., Wang, Y., Ma, X., Lu, H., and La, Z.: Observation and Process Understanding of Typical Cloud Holes Above Lakes Over the Tibetan Plateau, JGR Atmospheres, 128, e2023JD038617, https://doi.org/10.1029/2023JD038617, 2023.

Yau, M. K. and Rogers, R. R.: A short course in cloud physics, Elsevier, 1996.

Ye, D.: Some Characteristics of the Summer Circulation Over the Qinghai-Xizang (Tibet) Plateau and Its Neighborhood, Bull. Amer. Meteor. Soc., 62, 14–19, https://doi.org/10.1175/1520-0477(1981)062<0014:SCOTSC>2.0.CO;2, 1981.

https://doi.org/10.5194/egusphere-2026-869
Preprint. Discussion started: 9 April 2026
© Author(s) 2026. CC BY 4.0 License.



You, Q., Min, J., Lin, H., Pepin, N., Sillanpää, M., and Kang, S.: Observed climatology and trend in relative humidity in the central and eastern Tibetan Plateau, JGR Atmospheres, 120, 3610–3621, https://doi.org/10.1002/2014JD023031, 2015.

Zängl, G.: The impact of lee-side stratification on the spatial distribution of orographic precipitation, Q. J. R. Meteorol. Soc., 131, 1075–1091, https://doi.org/10.1256/qj.04.118, 2005.

Zhang, G., Yao, T., Xie, H., Zhang, K., and Zhu, F.: Lakes' state and abundance across the Tibetan Plateau, Chin. Sci. Bull., 59, 3010–3021, https://doi.org/10.1007/s11434-014-0258-x, 2014.

Zhang, G., Luo, W., Chen, W., and Zheng, G.: A robust but variable lake expansion on the Tibetan Plateau, Sci. Bull, 64, 1306–1309, https://doi.org/10.1016/j.scib.2019.07.018, 2019.

Zhang, X., Duan, K., Shi, P., and Yang, J.: Effect of lake surface temperature on the summer precipitation over the Tibetan Plateau, J. Mt. Sci., 13, 802–810, https://doi.org/10.1007/s11629-015-3743-z, 2016.

Zhao, P., Li, Y., Guo, X., Xu, X., Liu, Y., Tang, S., Xiao, W., Shi, C., Ma, Y., Yu, X., Liu, H., Jia, L., Chen, Y., Liu, Y., Li, J., Luo, D., Cao, Y., Zheng, X., Chen, J., Xiao, A., Yuan, F., Chen, D., Pang, Y., Hu, Z., Zhang, S., Dong, L., Hu, J., Han, S., and Zhou, X.: The tibetan plateau surface-atmosphere coupling system and its weather and climate effects: The third tibetan plateau atmospheric science experiment, J Meteorol Res, 33, 375–399, https://doi.org/10.1007/s13351-019-8602-3, 2019.

Zhao, Z., Huang, A., Ma, W., Wu, Y., Wen, L., Lazhu, and Gu, C.: Effects of Lake Nam Co and Surrounding Terrain on Extreme Precipitation Over Nam Co Basin, Tibetan Plateau: A Case Study, JGR Atmospheres, 127, e2021JD036190, https://doi.org/10.1029/2021JD036190, 2022.

Zheng, D., Fan, P., Zhang, Y., Yao, W., Fang, X., and Ran, R.: Deep convective clouds observed by ground-based radar over Naqu, Qinghai–Tibet Plateau, Atmospheric Research, 293, 106930, https://doi.org/10.1016/j.atmosres.2023.106930, 2023.